



Published in final edited form as:

Cell Metab. 2020 May 05; 31(5): 937–955.e7. doi:10.1016/j.cmet.2020.04.006.

Deamidation Shunts RelA from Mediating Inflammation to Aerobic Glycolysis

Jun Zhao¹, Mao Tian¹, Shu Zhang¹, Alireza Delfarah², Ruoyun Gao¹, Youliang Rao¹, Ali Can Savas¹, Anjie Lu³, Larissa Bubb¹, Xiao Lei⁴, Rosa Moshirian¹, Wenjie Zhu⁵, Cheng Peng³, Taijiao Jiang^{5,6}, Lin Chen⁴, Nicholas A. Graham², Pinghui Feng^{1,7,*}

¹Section of Infection and Immunity, Herman Ostrow School of Dentistry, Norris Comprehensive Cancer Center, University of Southern California, 925 W 34th Street, Los Angeles, CA 90089, USA

²Mork Family Department of Chemical Engineering and Materials Science, Norris Comprehensive Cancer Center, 3710 McClintock Avenue, Los Angeles, CA 90089, USA

³Department of Orthopedic and Plastic Surgery, The Third Xiangya Hospital of Central South University, Changsha, Hunan 410013, China

⁴Department of Molecular and Computational Biology, 1050 Childs Way, Los Angeles, CA 90089, USA

⁵Center of Systems Medicine, Institute of Basic Medical Sciences, Chinese Academy of Medical Sciences & Peking Union Medical College, Beijing 100005, China

⁶Suzhou Institute of Systems Medicine, Suzhou 215123, China

⁷Lead Contact

SUMMARY

Cell proliferation and inflammation are two metabolically demanding biological processes. How these competing processes are selectively executed in the same cell remains unknown. Here, we report that the enzyme carbamoyl-phosphate synthetase, aspartyl transcarbamoylase, and dihydroorotase (CAD) deamidates the RelA subunit of NF- κ B in cancer cells to promote aerobic glycolysis and fuel cell proliferation in tumorigenesis. This post-translational modification switches RelA function from mediating the expression of NF- κ B-responsive genes to that of glycolytic enzymes, thus shunting the cell's inflammatory response to aerobic glycolysis. Further, we profiled diverse human cancer cell lines and found that high CAD expression and a subset of *RELA* mutations correlated with RelA deamidation. And by use of inhibitors of key glycolytic

*Correspondence: pinghui@usc.edu.

AUTHOR CONTRIBUTIONS

Conceptualization, P.F. and J.Z.; Investigation, J.Z., M.T., S.Z., A.D., R.G., Y.R., A.C.S., A.L., L.B., X.L., R.M., and W.Z.; Writing – Original Draft, P.F., J.Z., L.C., and N.A.G.; Writing – Review & Editing, P.F., J.Z., and N.A.G.; Data Analyses, T.J.; Reagent Contribution, C.P.

SUPPLEMENTAL INFORMATION

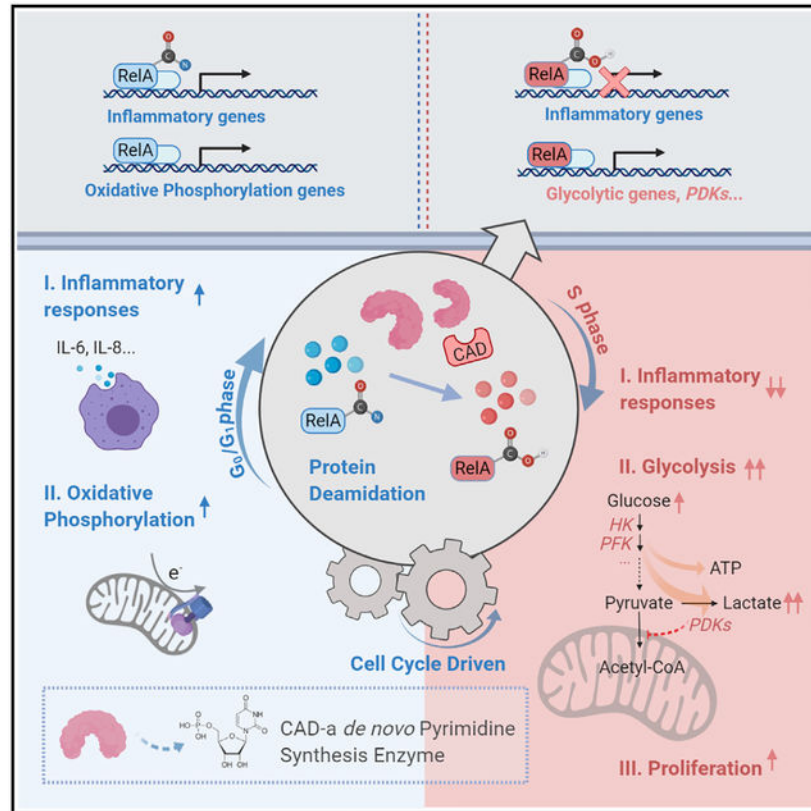
Supplemental Information can be found online at <https://doi.org/10.1016/j.cmet.2020.04.006>.

DECLARATION OF INTERESTS

The authors declare no competing interests.

enzymes, we validated the pivotal role of RelA deamidation in tumorigenesis of cancer cell lines. This work illuminates a mechanism by which protein deamidation selectively specifies gene expression and consequent biological processes.

Graphical Abstract



In Brief

CAD, the rate-limiting enzyme of the *de novo* pyrimidine synthesis pathway, deamidates RelA to promote aerobic glycolysis and cell proliferation at the expense of NF- κ B-dependent gene expression and an inflammatory response.

INTRODUCTION

Inflammation is a protective response to external insults such as tissue damage or microbial infection. Activated nuclear factor- κ B (NF- κ B) upregulates the expression of genes underpinning a broad spectrum of biological processes such as an immune response, inflammation, development, apoptosis, and tumorigenesis (Zhang et al., 2017). In response to microbial infection, pattern recognition receptors (PRRs) detect microbe-associated molecular patterns to induce the expression of inflammatory genes (Takeuchi and Akira, 2010). Localized in distinct anatomic cellular compartments, PRRs dimerize with their cognate adaptor molecules to activate two closely related kinases, the IKK and IKK-related TBK-1 complexes. IKK and TBK-1 activate NF- κ B and interferon regulatory factors (IRFs),

respectively (Seth et al., 2006). Activated NF- κ B, along with other transcription factors, drives the gene expression of immune function, establishing an antiviral inflammatory response that culminates in cytokine production (Sen and Baltimore, 1986).

Central to core cellular biological processes is the metabolic status of a cell. Mounting an inflammatory response and cell proliferation are two metabolically demanding processes that require dedicated metabolic machinery. Recent studies suggest the emerging theme that upon infection, a cell funnels its metabolic fluxes to support the initiation and sustenance of an inflammatory response that constitutes primarily a transcriptional pathway, resulting in the production of cytokines and chemokines (Mogilenko et al., 2019). In proliferating cells, metabolism is directed to support biomass accumulation in preparation for cell division (Locasale and Cantley, 2011). Although the coordination between metabolism and inflammation or metabolism and cell proliferation is well appreciated, these processes are primarily investigated in immune cells and cancer cells in isolation, respectively. How inflammation, such as that triggered by innate immune activation, and cell proliferation are coordinated in the same cell remains elusive. For example, it has been observed that immune activation is often suppressed, particularly in S phase of cycling cells, yet how such cell cycle regulation is achieved is unclear (Ankers et al., 2016).

Glutamine amidotransferases (GATs) constitute a family of metabolic enzymes that extract nitrogen from glutamine to synthesize nucleotides, amino acids, glycoproteins, and the enzyme cofactor nicotinamide adenine dinucleotide (NAD), which are building blocks for cell growth and proliferation (Massière and Badet-Denisot, 1998). In mammals, the trifunctional enzyme carbamoyl-phosphate synthetase, aspartyl-transcarbamoylase, and dihydroorotase (CAD) catalyzes the first three sequential steps of *de novo* pyrimidine synthesis (Shoaf and Jones, 1973). The first step of carbamoyl-phosphate synthesis is rate limiting for *de novo* pyrimidine synthesis, endowing CAD with diverse regulatory mechanisms. In response to growth factor stimulation, CAD is phosphorylated and activated by MAP (mitogen-activated protein) kinase (Graves et al., 2000) and S6K (Ben-Sahra et al., 2013; Robitaille et al., 2013) to promote pyrimidine synthesis and facilitate subsequent cell proliferation. Our understanding of the role of CAD is limited to its enzymatic activity in catalyzing *de novo* pyrimidine synthesis. We reported here that CAD functions as a RelA deamidase. RelA (also known as p65) is the transcriptionally active subunit of the prototype NF- κ B dimer containing RelA and p50 (Nolan et al., 1991; Sen and Baltimore, 1986). Activated NF- κ B transactivates the expression of a large array of inflammatory genes, including cytokines and chemokines. We found that CAD deamidates RelA and diminishes NF- κ B activation in a cell cycle-dependent manner. Moreover, CAD-deamidated RelA promotes aerobic glycolysis and inhibits mitochondrial oxidative phosphorylation via activating the expression of key glycolytic enzymes to fuel cell proliferation. This study describes a nonmetabolic activity (*i.e.*, deamidation) of a nucleotide-synthesizing enzyme in promoting aerobic glycolysis and suppressing inflammation, and one that underpins the proliferation and tumorigenesis of diverse human cancer cell lines.

RESULTS

Identification of CAD as a Negative Regulator of NF- κ B Activation

Our previous studies showed that a cellular GAT deamidates RIG-I to avoid antiviral cytokine production, suggesting that GATs can regulate fundamental biological processes via deamidation. To test this idea, we performed a focused screen to assess NF- κ B activation when cellular GATs were depleted with short hairpin (sh)RNA as we recently reported (Li et al., 2019). The human genome encodes 11 GATs participating in the synthesis of nucleotides, amino acids, glycoproteins, and NAD (Figure S1A). The screen demonstrated that knockdown of CAD significantly increased NF- κ B activation by reporter as-says (Figure 1A). Further analysis indicated that depletion of CAD consistently increased the expression of NF- κ B-responsive genes, such as *IL-8*, in 293T cells in response to Sendai virus (SeV) infection or TNF- α treatment (Figures 1B and S1B). Similar results were obtained in CAD-depleted human THP-1 monocytes and BJ5 fibroblasts upon SeV infection (Figures 1C and S1C). Furthermore, we generated CAD knockout 293T cells via CRISPR-Cas9 and found that CAD knockout resulted in greater *ICAM1* and *IL-8* gene expression versus wild-type cells (Figure 1D). The greater gene expression correlated with elevated cytokine production in THP-1 cells upon SeV infection or lipopolysaccharide (LPS) treatment (Figure 1E). Finally, CAD depletion in colorectal HCT116 cells also led to greater *IL-8* gene expression in response to *Salmonella typhimurium* infection (Figures S1D and S1E) versus normal cells. Interestingly, *Salmonella typhimurium* infection modestly induced the expression of CAD, but not that of the other GATs, in HCT116 cells (Figure S1F).

To determine the specificity of CAD in NF- κ B activation, we found that CAD depletion did not significantly increase the IFN- β reporter expression (Figure S1G). Though CAD knockdown may reduce intracellular pyrimidine concentration, supplementing CAD-depleted HCT116 cells with uridine had no effect on NF- κ B activation in 293T cells (Figure S1H). Furthermore, knockdown of UMP synthetase (UMPS), an enzyme downstream of CAD, had no effect on SeV-induced NF- κ B activation (Figure S1I). These results show that CAD negatively regulates NF- κ B activation independent of pyrimidine synthesis.

CAD Deamidates RelA to Inhibit NF- κ B Activation

CAD demonstrates an inhibitory effect on NF- κ B activation that can be triggered by multiple physiological stimuli, which engage distinct cellular receptors and converge at the downstream IKK kinase (Figure 1F), suggesting that CAD acts on a component(s) of the shared portion of the NF- κ B pathway. Indeed, CAD knockdown resulted in greater NF- κ B activation induced by the ectopic expression of all components of the RIG-I-NF- κ B pathway, including the constitutively active N-terminal caspase activation and recruitment domains (CARDs) (RIG-I-N), MAVS, IKK β , and RelA (Figure 1G), whereas overexpression of CAD inhibited NF- κ B activation (Figures S1J and S2A). These results suggest that CAD likely targets RelA to diminish NF- κ B activation.

To test whether the glutamine amidotransferase activity is important for the inhibition of NF- κ B activation, we created an enzyme-deficient mutant of CAD in which the active site, cysteine 252 (C252), was replaced with serine, designated CAD-C/S. Reporter assays

indicated that wild-type CAD potently, while CAD-C/S mutant marginally, diminished NF- κ B activation in a dose-dependent manner (Figure 2A). We then examined whether CAD interacted with RelA and found that endogenous CAD and RelA were readily co-precipitated in 293T cells (Figure S2B). By contrast, CAD failed to co-precipitate with RelB and cRel (Figure S2C). The residual p50 precipitated by CAD is likely due to the RelA subunit that interacts with both p50 and CAD. Mutational analysis indicated that the N-terminal domain (amino acids 1 to 311) of RelA is sufficient and necessary to interact with CAD in transfected 293T cells (Figure S2D).

To assess whether CAD deamidates RelA, we monitored the charge status of RelA by two-dimensional gel electrophoresis (2DGE) upon CAD depletion in human HCT116 cells. In control HCT116 cells, two distinct species of RelA were detected (Figure 2B). When CAD was depleted with shRNA, the more negatively charged species was greatly reduced, indicative of diminished deamidation (Figure 2B). Endogenous RelA was highly deamidated in transfected 293T cells, while overexpressed CAD further deamidated RelA and depleted the undeamidated species without altering the charge status of p50 (Figure S3A), indicating the specificity of CAD-mediated RelA deamidation. Medium from CAD-knockdown cells did not suppress RelA deamidation, indicating that the intrinsic deamidase activity of CAD is required to deamidate RelA in a cell autonomous manner (Figure S3B). We then purified RelA with or without exogenously expressed CAD and analyzed RelA post-translational modifications by tandem mass spectrometry. This analysis identified two sites, asparagine 64 and 139, that experienced an increase in deamidation with CAD expression (Figures S3C and S3D). To assess the specificity of the deamidation, we generated a RelA mutant that contains two N>D mutations (i.e., N64D and N139D), referred to as RelA-DD. Exogenous expression of CAD shifted wild-type RelA, but not RelA-DD, toward the positive side of the gel strip (Figure S3E). This result suggests that there are no additional sites within RelA that can be deamidated by CAD.

To test whether CAD is a bona fide deamidase, we purified GST-RelA, CAD, and the enzyme-deficient CAD-C/S mutant to high homogeneity (Figure 2C, left panel) and performed an *in vitro* deamidation assay. Purified GST-RelA demonstrated two species by 2DGE, with a minor species migrating toward the positive side of the strip (Figure 2C). Compared to the control reaction, CAD shifted RelA toward the positive end of the gel strip, yielding two more new species compared to the control reaction (Figure 2C). Importantly, the CAD-C/S mutant did not shift RelA, and the glutamine amidotransferase inhibitor DON (500 nM) significantly reduced the amount of the two new species that were engendered by CAD. These results show that CAD deamidates RelA in cells and *in vitro*.

RelA is one of the most extensively studied members of the Rel family of transcription factors that share a conserved rel homology domain (RHD, Figure 2D). The crystal structure of RelA RHD has been solved in various complexes including the Rel homodimer bound to DNA (PDB code: 1RAM) (Chen et al., 1998). The two deamidation sites are both located within the RHD-N subdomain of RelA, which has a typical beta-sandwich structure. One of the deamidation sites, N64, is located on the β_B - β_C Loop, whereas the other deamidation site, N139, is located on the so-called “insertion region” of RelA. Both sites are far away from the DNA-binding and dimerization interfaces, providing no clear indication concerning

how deamidation impacts RelA function (Figure 2D). Thus, we used the deamidated RelA-DD mutant to determine the effect of deamidation on NF- κ B-dependent gene expression. Reporter assays indicated that single deamidation mutants, RelA-64D and RelA-139D, were partly impaired in their abilities to activate NF- κ B. Remarkably, the RelA-DD mutant showed residual activity to activate the NF- κ B promoter (Figure S3F). These RelA mutants were expressed at levels similar to that of wild-type RelA. We have also generated RelA mutants containing N64A (RelA-64A) and N139A (RelA-139A) mutations. While RelA-139A was impaired in its capacity to activate NF- κ B, RelA-64A more potently activated the NF- κ B promoter than wild-type RelA (Figure S3G and data not shown). Consistent with that, RelA-64A was more resistant to CAD-mediated deamidation, assessed by 2DGE and inhibition by reporter assays, than wild-type RelA (Figures S3H and S3I).

To gain insight into the role of deamidation in RelA-mediated gene expression, we first reconstituted RelA-deficient (*Rela*^{-/-}) mouse embryonic fibroblasts (MEFs) with wild-type RelA or the deamidated RelA-DD (Figure 2E, top panel) and analyzed the expression of a few known NF- κ B-responsive genes. This analysis showed that SeV infection potently induced the expression of NF- κ B-responsive genes in *Rela*^{-/-} MEFs reconstituted with wild-type RelA, but failed to induce the expression of *Mip2* and *Tnfa* and only weakly induced that of *Ccl5* in cells reconstituted with RelA-DD (Figure 2E). RNA sequencing analysis further showed that, upon SeV infection, NF- κ B-dependent genes were among the most significantly reduced in gene expression in *Rela*^{-/-} MEFs reconstituted with RelA-DD (Figure 2F). Furthermore, we introduced N64D and N139D mutations into the *Rela* locus of BL6 mouse, designated RelA-DD knockin (Figure S4A). We isolated primary MEFs and found that SeV infection induced significantly lower expression of *Cxcl-1*, *Il-8*, and *Tnfa* (Figure S4B). Finally, RelA-depleted HCT116 cells reconstituted with wild-type RelA and RelA-DD (Figure S4C) recapitulated the differential expression profile of NF- κ B-dependent genes (Figure S4D), while RelA-64A more robustly upregulated NF- κ B-dependent gene expression than wild-type RelA. These results show that deamidation impairs the transcriptional activation of NF- κ B-dependent genes by RelA.

To probe the molecular mechanism by which deamidation negatively impacts RelA-mediated NF- κ B activation, we analyzed the interaction with I κ B α and p50 and the nuclear translocation of RelA. CoIP assays showed that, compared to wild-type RelA, RelA-DD and RelA-64A showed comparable and reduced interactions with I κ B α , respectively (Figure S4E). Fractionation of nuclei and cytoplasm indicated that RelA-DD accumulated in the nucleus with similar kinetics as wild-type RelA upon TNF- α treatment (Figure S4F). By contrast, compared to wild-type RelA, RelA-DD and RelA-64A demonstrated lower and higher interaction with p50, respectively (Figure 2G). The same pattern of p50 interaction was observed in these reconstituted HCT116 cells under mock and TNF- α -treated conditions (Figure S4G). When CAD was depleted in 293T cells, more p50 was precipitated with RelA in resting and SeV-infected cells, supporting that CAD-mediated deamidation negatively regulates RelA interaction with p50 (Figure 2H). The p50-interacting activity of these RelA proteins correlated well with their ability to activate NF- κ B. This result agrees with the observation that the p50-RelA dimer has the highest affinity for the promoter of NF- κ B-responsive genes (Phelps et al., 2000). To test the regulatory role of CAD on p50-mediated NF- κ B induction, we engineered p50-deficient 293T cells for SeV infection. Real-

time analysis indicated that CAD depletion had minimal effect on the induction of NF- κ B-dependent gene expression in p50-deficient cells (Figures S4H and S4I). This result indicates that CAD negatively regulated NF- κ B-dependent gene expression mediated by the p50-p65 complex. We further performed a ChIP assay to probe the promoter-associated RelA using reconstituted HCT116 cells. This analysis demonstrated that wild-type RelA, but not RelA-DD, precipitated a significant amount of DNA of the promoter sequences of *TNFA*, *IKBA*, and *IL-8* (Figure S4J). These results show that deamidation impairs the ability of RelA to interact with p50, which recruits RelA to the promoter of NF- κ B-responsive genes.

RelA Deamidation and Reduced Expression of NF- κ B-Responsive Genes Are Cell Cycle-Dependent

In proliferating cells, CAD is activated in S phase to promote nucleotide synthesis in preparation for DNA replication (Sigoillot et al., 2003). To probe the deamidase activity of CAD during cell proliferation, we analyzed RelA deamidation in synchronized cycling cells. HCT116 cells were arrested by lovastatin at G1 phase and released for cell cycle progression, validated by immunoblotting analyses of cyclins E, A, and B (Figures 3A and 3B). Analysis of RelA by 2DGE indicated that RelA deamidation peaked at 20 h after release, which corresponded to late S phase and quickly diminished thereafter (Figure 3C). The enzymatic activity in pyrimidine synthesis of CAD is activated by phosphorylation of serine 1859 (S1859) mediated by S6K (Ben-Sahra et al., 2013; Robitaille et al., 2013). We thus engineered HCT116 cells expressing a Flag-epitope at the carboxyl-terminus of the endogenous CAD, which allowed us to purify CAD for *in vitro* biochemical analysis. We first analyzed CAD phosphorylation and found CAD phosphorylation (S1859) peaked at 20 h and remained high from 16 to 24 h after release from lovastatin (Figure 3D). When purified CAD was analyzed by *in vitro* RelA deamidation, we observed that the RelA-deamidating activities paralleled the phosphorylation of S1859 (Figure 3E). We also treated cells with double thymidine, which arrests cells in S phase (Figure S5A), and analyzed RelA deamidation after release. This analysis showed that a large fraction of RelA was deamidated in S phase and that this fraction diminished when cells exited from S phase (Figure S5B). The phosphorylation of S1859 of CAD also correlated with the level of deamidated RelA (Figures S5B and S5C). These results suggest that the deamidase activity of CAD is high during S phase, likely concurrent with its pyrimidine-synthesizing activity.

Concomitant with RelA deamidation, the expression levels of NF- κ B-dependent genes were downregulated with the progression into S phase. The downregulation of *IL-6* and *IL-8* expression showed quick and robust kinetics paralleling RelA deamidation, compared to the slow downregulation of *ICAM1* expression (Figure 3F). Moreover, SeV-induced *IL-8* expression inversely correlated with RelA deamidation during cell cycle; i.e., *IL-8* expression peaked at 6 h after double thymidine release when RelA deamidation was the lowest (Figure S5D). In stark contrast, the expression of four interferon-related genes, i.e., *IFN β* , *DDX60*, *IRF7*, and *IFI44*, increased gradually with the progression of cell cycle (Figure 3G). In BJ5 fibroblast cells, the expression of these two categories of genes segregated during cell cycle (Figures S5E and S5F). We further validated the lower NF- κ B activation in S phase by RNA sequencing analysis using HCT116 cells synchronized in G1

and S phase. This analysis showed that the expression levels of NF- κ B-dependent genes, including *SERPINE1*, *IL-18*, *IL-6R*, and the TNFR superfamily (*TNFRSF1A*, *12A*, and *21*), were downregulated in S phase (Figure 3H), but those of interferon-related genes (*IFI44*, *IRF7*, and *MX2*) were not (Figure S5G). Thus, NF- κ B activation is suppressed during S phase via RelA deamidation.

To probe the role of CAD in inhibiting NF- κ B activation in S phase, we introduced RelA-64A and wild-type RelA into HCT116 cells and analyzed the expression of *IL-6*, *ICAM1*, and *IL-8*. Remarkably, RelA-64A, compared to wild-type RelA, led to greater *IL-6* and *ICAM1* expression in S phase, while it sustained *IL-8* expression (Figure S5H). The expression of all three genes was downregulated in HCT116 cells expressing wild-type RelA. Furthermore, we depleted CAD expression with shRNA and examined the expression of NF- κ B-dependent genes. CAD knockdown in HCT116 cells (Figure S6A) resulted in slightly higher *EGR1* expression and much higher *ICAM1* expression in S phase versus control cells (Figure S6B). Thus, knockdown of CAD or ectopic expression of the deamidation-resistant RelA-64A mutant lead to greater expression of NF- κ B-dependent genes in S phase.

To determine whether CAD-mediated RelA deamidation is regulated during innate immune activation, we monitored RelA charge change upon LPS treatment or SeV infection. Compared to the mock-treated group, the deamidated species of RelA was detectably reduced in LPS-treated or SeV-infected groups (Figure S6C). Consistent with NF- κ B activation, LPS treatment and SeV infection increased RelA phosphorylation of serine 536. Furthermore, using the Flag-tagged CAD HCT116 cells, we affinity-purified CAD from mock-treated, LPS-treated, and SeV-infected cells and carried out *in vitro* RelA deamidation assay. This analysis indicated that LPS treatment and SeV infection inhibited the deamidase activity of CAD (Figure S6D). These results indicate that CAD-mediated RelA deamidation is negatively regulated by signals to activate NF- κ B.

Deamidated RelA Promotes Aerobic Glycolysis and Cell Proliferation

While culturing HCT116 cells, we observed that the medium of RelA-depleted cells reconstituted with RelA-DD turned yellow much sooner than that of cells reconstituted with wild-type RelA or RelA-64A. Quantification of lactate production from these cells showed that the reconstituted expression of RelA-DD and wild-type RelA, but not that of RelA-64A, resulted in higher lactate production by ~70% and ~30%, respectively (Figure S7A). Extracellular acidification rate (ECAR) analysis further showed that HCT116 cells reconstituted with RelA-DD generated much more lactate than those expressing wild-type RelA and RelA-64A (Figure 4A). Glucose uptake analysis using 2-deoxyglucose (2-DG) indicated that RelA-DD increased glucose uptake by ~40%, while RelA-64A reduced it by ~30% (Figure 4B). Similarly, RelA-DD knockin MEFs demonstrated significantly higher glucose consumption and lactate production compared to wild-type MEFs (Figures S7B and S7C). In contrast, the oxygen consumption rate (OCR) showed that RelA-64A resulted in much greater mitochondrial respiration and that wild-type RelA did so to a lesser extent (Figure 4C), while RelA-DD induced a smaller, but detectable, increase. These results

suggest that RelA deamidation switches cellular metabolic program from mitochondrial oxidative phosphorylation to aerobic glycolysis.

Next, we determined whether CAD had effects similar to RelA-DD. Depletion of CAD in HCT116 cells significantly reduced lactate production (Figure 4D). Moreover, HCT116 cells synchronized to S phase also demonstrated elevated ECAR, and shRNA-mediated depletion of CAD abolished the increase in extracellular acidification of S phase HCT116 cells (Figure S7D). In contrast, synchronizing HCT116 cells to S phase reduced OCR, and knockdown of CAD abolished the reduction of OCR induced by S phase synchronization (Figure 4E). CAD depletion also led to a slightly higher OCR in unsynchronized HCT116 cells, likely due to the small percentage of cells cycling in S phase. Furthermore, the expression of RelA-64A, but not that of wild-type RelA, abolished the increase in EACR induced by S phase synchronization (Figure S7E) that correlated with elevated OCR (Figure S7F). These results support the conclusion that CAD-mediated RelA deamidation suppresses mitochondrial oxidative phosphorylation and promotes glycolysis.

To assess the biological significance of RelA deamidation, we examined cell proliferation and tumorigenesis of RelA-depleted HCT116 cells reconstituted with wild-type and mutant RelA. In RelA-depleted HCT116 cells, reconstituted expression of wild-type RelA and RelA-DD resulted in significantly greater cell proliferation, while that of RelA-64A had no detectable effect (Figure 4F). Similarly, expression of RelA-DD, but not that of RelA-64A, in RelA-depleted SW480 colorectal cancer cells led to greater lactate production and cell proliferation (Figures S7G and S7H). To determine the role of CAD in deamidating RelA and promoting cell proliferation, we depleted CAD and ectopically expressed RelA-DD in HCT116 cells (Figure S7I). Not surprisingly, CAD depletion impaired the proliferation of HCT116 cells, and expression of RelA-DD partly restored the proliferation (Figure S7J). Consistent with this, expression of wild-type RelA in RelA-knockdown HCT116 cells resulted in greater population of S phase cells from 6% to 13%, and RelA-DD increased the S phase population to 15%, whereas RelA-64A had no effect (Figure 4G). Cells in G2 and M phase were 11% and 15% in cells expressing wild-type RelA and RelA-DD, respectively, and it was 8% in those expressing RelA-64A. When these reconstituted HCT116 cells were subcutaneously transplanted into nude mice, we found that RelA-DD, and to a lesser extent wild-type RelA, potently promoted tumor formation, as assessed by tumor size (Figure S7K) and weight (Figures 4H and S7L). Notably, RelA-64A also yielded slightly greater tumors versus control, likely due to its inhibition of apoptosis. Lactate production from tumors derived from these reconstituted cell lines also correlated with their ability to promote tumor formation (Figure 4I). These results collectively show that deamidated RelA promotes cell proliferation and tumor growth.

Deamidated RelA Programs Metabolism via Regulating Gene Expression

We analyzed RNA sequencing data derived from RelA knockdown HCT116 cells reconstituted with wild-type RelA, RelA-DD, and RelA-64A. This data identified a subset of metabolic enzymes that were differentially regulated by RelA-DD and RelA-64A (Figure 5A). Notably, these enzymes cluster into the glycolysis, pentose phosphate pathway, nucleotide biosynthesis, and tricarboxylic acid (TCA) cycle. Real-time PCR analysis

focusing on key glycolytic enzymes and transporters revealed that the expression of glucose transporter (Glut3), hexokinases (HK2 and 4), phosphofructose kinases (PFKP, PFKM, and PFKL), pyruvate dehydrogenase kinases (PDK1, 2, and 3), pyruvate carboxylase (PC) and glutamate-pyruvate transaminase (GPT) were induced by RelA-DD and wild-type RelA, but not RelA-64A (Figures 5B and S8A). When compared to wild-type RelA, RelA-DD similarly induced the expression of PFK (P, M, and L) and PK (M1, M2, and LR) and more potently induced Glut3, HK4, and PDK3 (Figure S8A). RelA-64A either failed to induce or only weakly induced most of these enzymes, indicating the promoter specificity of deamidated RelA. Interestingly, PK (M1 and M2) and LDH (A and B) were equally induced by wild-type RelA, RelA-DD, and RelA-64A (Figure S8A). Immunoblotting analysis indicated that RelA-DD elevated the protein levels of PC, PDK2, PDK3, HK4, and PFKP, while wild-type RelA had modest effects and RelA-64A had no effect on their protein expression (Figure 5C). Consistent with the upregulation of PDK by RelA-DD, the phosphorylation of serine 293 of pyruvate dehydrogenase α subunit (PDHA1) was readily detected in cells reconstituted with RelA-DD. In CAD-depleted cells, reconstituted expression of RelA-DD restored the expression of PC, PDK2, and PFKP (Figure S8B). On the other hand, RelA-DD induced lower levels of expression of components of the mitochondrial respiration chain compared to wild-type RelA and RelA-64A, including those of the ATP synthase, complex I, III, and IV (Figure 5D). Thus, the deamidated RelA-DD and deamidation-resistant RelA-64A preferentially upregulate the expression of key glycolytic enzymes and mitochondrial respiration components, respectively.

To probe the role of CAD in glycolytic enzyme expression during cell cycle, we synchronized HCT116 cells with lovastatin (Figure S8C) and analyzed the expression of a few representative enzymes, including PDKs, PFKP, PC, and HK4. Real-time analysis indicated that all enzymes demonstrated cell cycle-dependent induction peaking at 20 h after release, concurrent with the peak RelA deamidation in late S phase (Figures S8D and S8E). Robust induction was observed for PDK2, PFKP, and PC, while modest or weak induction was observed for the rest of the tested genes. The induction of these glycolytic genes by RelA-DD, and to a lesser extent by wild-type RelA, was also observed in tumors derived from reconstituted HCT116 cell lines (Figure S8F). The upregulation of glycolytic genes by RelA-DD was further validated by chromatin immunoprecipitation and real-time PCR analysis that RelA-DD showed 2- to 4-fold higher binding to the promoters of GLUT3, HK4, PFKP, PDK2, and PDK3 in reconstituted HCT116 cells (Figure S8G). Finally, primary RelA-DD knockin MEFs have significantly higher expression of glycolytic genes compared to wild-type MEFs (Figure S8H). Thus, the induction of glycolytic enzymes parallels CAD-mediated RelA deamidation in a cell cycle-dependent manner.

To validate the function of upregulated glycolytic enzymes, we analyzed the intracellular concentrations of key intermediates of the glycolytic pathway in reconstituted HCT116 cells. We found that RelA-DD expression resulted in greater amount of nearly all intracellular metabolites of the glycolytic pathway, compared to RelA-64A (Figure 5E). These metabolites include glucose, fructose 1,6-bisphosphate (F1,6BP), dihydroxyacetone phosphate (DHAP), 3-phosphoglycerate (3-PG), 2-phosphoglycerate (2-PG), phosphoenol pyruvate (PEP), pyruvate, and lactate. Compared to wild-type RelA and RelA-64A, RelA-DD led to greater concentration of intracellular metabolites in the lower portion of the

glycolysis pathway, such as 3-PG, 2-PG, PEP, and pyruvate. Wild-type RelA demonstrated an intermediate phenotype with moderately higher intracellular glycolytic metabolites. Additionally, RelA-DD led to higher intracellular concentrations of acetyl-CoA, citrate, isocitrate, aconitate, and α -ketoglutarate (Figure S8I). These metabolites constitute the so-called reductive carboxylation pathway, which shunts carbon from glutamine to fatty acid synthesis (Metallo et al., 2011). Finally, RelA-DD also resulted in greater nucleotide levels, particularly ADP, GDP, CDP, UDP, and UTP, compared to RelA-64A (Figure S8J), suggesting the upregulation of the pentose phosphate pathway.

To monitor the activity of the glycolytic pathway, we determined the intracellular accumulation of glucose-derived carbon in lactate after feeding reconstituted HCT116 cells with isotope-labeled [U- 13 C]glucose (Figure 5F). At 15 min after isotope addition, RelA-DD resulted in greater lactate labeling up by \sim 70%, while wild-type RelA did to a lesser extent and RelA-64A had a marginal effect (Figure 5G). The accumulation of intermediates of the lower portion of the glycolytic pathway suggests the flux of glycolytic metabolites into its branched pathways, such as the serine-glycine pathway (Figure 5F). Thus, we determined glycolytic serine synthesis with the isotope-labeled [U- 13 C]glucose. Indeed, RelA-DD and wild-type RelA resulted in greater glycolytic serine synthesis by 120% and 60%, respectively, while that of RelA-64A did the opposite (Figure 5H).

To assess the activity of PC that converts pyruvate into oxoacetate and subsequently malate (Figure 5I), we labeled reconstituted HCT116 cells with [1- 13 C]pyruvate and determined the level of M+1 malate, which indicates flux from pyruvate. Consistent with the upregulated expression of PC, RelA-DD led to greater amount of M+1 malate (up by \sim 33%), while wild-type RelA and RelA-64A had the opposite effect (down by \sim 33%) (Figure 5J). Interestingly, wild-type RelA and RelA-64A resulted in lower intracellular citrate (isocitrate) labeling by \sim 40%, whereas RelA-DD had no effect (Figure 5J). The reduction in malate and citrate (isocitrate) labeling from pyruvate is likely due to elevated NF- κ B activation and subsequent oxidative phosphorylation via TCA cycle. These results collectively show that RelA-DD promotes, while RelA-64A inhibits, flux from glucose to lactate, serine, and malate.

RelA Deamidation Underpins the Elevated Glycolysis of Diverse Cancer Cell Lines

CAD-mediated RelA deamidation promotes glycolytic metabolism and cell proliferation, implying its contribution to tumorigenesis. We assessed CAD expression, RelA deamidation, glycolytic gene expression, and lactate production of a panel of human cancer cell lines that originate from the lung, colorectum, breast, head, and neck. In general, CAD expression correlated well with RelA deamidation in these diverse cell lines (Figures 6A and S9A). Specifically, cell lines with high CAD expression and high deamidated RelA included MCF7, MDA-MB-231, SW480, HCT116, HT29, H522, H358, H1648, and H23 (Figure S9A). Importantly, RelA deamidation correlated with upregulated expression of glycolytic genes and lactate production in these cancer cell lines (Figures 6B, 6C, and S9B). Of head and neck cancer cells, D562 and SCC-15 demonstrated high RelA deamidation and high glycolytic gene expression (Figures S9C and S9D). To probe the role of RelA deamidation in programming aerobic glycolysis, we ectopically expressed wild-type RelA, RelA-DD, and RelA-64A in cancer cell lines that showed no detectable deamidated RelA and low

lactate production. These included two colorectal (DLD-1 and LoVo), one breast (T47D), and one lung (H1975) cancer cell line (Figure S9A). In DLD-1 cells, RelA-DD induced the expression of key glycolytic enzymes, including PDKs, HK4, PC, and PFKP, while RelA-64A upregulated the expression of IL-8 (Figure 6D). The induction of these glycolytic enzymes by RelA-DD was substantiated by elevated lactate production (Figure 6E). Similarly, RelA-DD, but not RelA-64A, induced the expression of PDK2 and PDK3 and resulted in greater lactate production up by >110% in LoVo cells (Figures S9E and S9F), which also correlated with a higher cell proliferation rate (Figure S9G). In T47D breast and H1975 lung cancer cells, RelA-DD upregulated the expression of glycolytic genes, while RelA-64A induced IL-8 expression (Figures S10A and S10B). In RelA-depleted SW480 cells, RelA-DD upregulated the expression of HK4, PDK3, PC, and PFKP, while RelA-64A activated that of IL-8 as well as PC, PFKP, and HK4 (Figure S10C). These results show that deamidated RelA, but not deamidation-resistant RelA-64A, upregulates glycolytic gene expression.

Next, we tested whether the glycolysis elevated by deamidated RelA renders these cells sensitive to glycolytic inhibitors. To test this idea, we first applied 2-DG to reconstituted HCT116 cell lines. We found that RelA-DD and wild-type RelA sensitized HCT116 cells to 2-DG, while RelA-64A had no apparent effect (Figure 6F). Using a panel of 24 cancer cell lines, we profiled their sensitivity to 2-DG by determining cell growth. This analysis showed that cell lines with high RelA deamidation also demonstrated high sensitivity to 2-DG (Figures 6G and S10D). On the other hand, cell lines with low RelA deamidation were generally resistant to 2-DG treatment. Similar results were obtained with PFK158 (Clem et al., 2013), an inhibitor of PFKFB3 (Figures S10E and S10F). These results indicate that CAD-mediated RelA deamidation is crucial for the glycolytic metabolism and proliferation of cancer cells.

To further explore the role of RelA deamidation in tumorigenesis, we determined whether cancer cells with high RelA deamidation are more sensitive to PFK158, a PFKP inhibitor, in nude mice than those with low RelA deamidation. We chose three human colorectal cancer cell lines, two with high RelA deamidation (HCT116 and HT29) and one with low RelA deamidation (LoVo). These cells were transplanted into nude mice and PFK158 was applied every 3 days. Remarkably, PFK158 reduced the growth rate of tumors derived from HCT116 and HT29 cells by ~80% and ~75%, respectively (Figure 6H). This was further supported by final tumor weight (Figures 6I and S10G). By contrast, PFK158 had no significant effect on the growth or weight of tumors derived from LoVo cells (Figures 6H, 6I, and S10G). In conclusion, RelA deamidation correlates with sensitivity to inhibitors of glycolytic enzymes in cancer cells.

A Subset of Cancer-Associated Mutations Render RelA Highly Deamidated and the Ability to Promote Glycolysis and Fuel Cell Proliferation

NF- κ B transcription factors are implicated in oncogenesis, most notably for their function in provoking inflammation and resisting apoptosis, although opposing activities in tumorigenesis were reported (Perkins, 2004). Our study showed that deamidated RelA predisposes cells to aerobic glycolysis and fuels cell proliferation, suggesting its contribution

to carcinogenesis. Mutations in the *RELA* gene are found in a number of human cancers, but their roles in tumorigenesis have not yet been characterized (Figure 7A). Exploring the human TCGA (The Cancer Genome Atlas) dataset, we focused on those mutations that cluster in the Rel homology domain. We introduced these mutations into human RelA and examined NF- κ B activation by reporter assays. We reasoned that mutations impairing NF- κ B activation likely give RelA new functions, e.g., glycolytic reprogramming. An NF- κ B reporter assay identified a panel of mutations that partly or severely impair NF- κ B activation of RelA (Figure 7B). Mutations of R33H, R187C, V199A, E211K, or I250V partly impaired, while mutations of G208S, G209V, D243Y, P256L, or S276F abolished, NF- κ B activation (Figure 7C). These RelA mutants were expressed in LoVo cells that have low RelA deamidation to assess their deamidation status. RelA mutants containing R187C, V199A, G209V, and E211K showed higher deamidation as analyzed by 2DGE (Figure 7D). Moreover, the expression of these four RelA mutants in RelA-depleted HCT116 cells induced the expression of HK4, PFKF, PDK2, and PDK3, and the production of lactate (Figures 7E and 7F). The RelA R33H mutant, although with low deamidation, upregulated the expression of glycolytic enzymes and promoted lactate production via unknown mechanisms likely independent of RelA deamidation. The increase in glycolytic metabolism also correlated with elevated cell proliferation (Figure 7G). Finally, these RelA mutants promoted tumor formation in nude mice, indicative of their growth-promoting activity *in vivo* (Figure 7H). Collectively, these results indicate that a subset of RelA mutations endow RelA with glycolysis-promoting activity, fueling cell proliferation and tumor progression.

DISCUSSION

Key cellular biological processes are often coupled to the metabolic status of a cell. Our understanding of how metabolism is tailored for distinct bioprocesses, such as immune responses, cell replication, and transformation, has advanced significantly in the past two decades, specifically from studies using immune and cancer cells. However, how distinct metabolically demanding bioprocesses, such as an inflammatory response and cell proliferation, are coordinated in the same cell remains poorly defined. We report here that during cell cycle progression, CAD-mediated RelA deamidation shuts down NF- κ B-mediated proinflammatory responses, whereas aerobic glycolysis is promoted to fuel cell proliferation. Our study uncovers a mechanism by which cells funnel energy and metabolic flux to support replication; namely, via deamidation of a key transcription factor to specify downstream gene expression.

CAD Is a Bona Fide Protein Deamidase

To date, CAD has been studied for its activity in *de novo* pyrimidine synthesis that supports the increased need for nucleotides during cell proliferation (Sigoillot et al., 2003). We report here that CAD also programs cellular metabolism via deamidating RelA, thus driving the expression of key metabolic enzymes, particularly those of the glycolytic pathway. This study identifies CAD as a genuine deamidase that is sufficient to deamidate RelA *in vitro* and in cells, supporting the hypothesis that cellular GATs are intrinsically protein deamidases in metazoans. In synchronized cells, RelA deamidation peaks in late S phase, when CAD is known to be active in catalyzing pyrimidine synthesis, suggesting that the

deamidase activity of CAD parallels its nucleotide-synthesizing activity in cell proliferation. Conceivably, both the activity in pyrimidine synthesis and ability to promote glycolysis via deamidation of RelA by CAD are required for anabolism in S phase and cell proliferation. Aerobic glycolysis driven by CAD-mediated RelA deamidation supplies glycolytic intermediates for nucleotide synthesis, setting up the stage for CAD-mediated pyrimidine synthesis.

Our study on the deamidase activity of CAD supports the emerging theme that metabolic enzymes can assume a nonmetabolic function. For example, glycolytic enzymes are originally known to act on central carbon metabolites, which are small molecules in nature. However, pyruvate kinase M2 (PKM2) has been recently shown to localize to the nucleus and phosphorylate histone H3 (Yang et al., 2012), thereby regulating gene expression via epigenetic modification. An *in vitro* screen using protein micro-assay identified more than 100 human proteins that can be phosphorylated by PKM2, suggesting more regulatory roles of PKM2 beyond metabolism (He et al., 2016). HK1 can autophosphorylate and phosphorylate histone H2A (Adams et al., 1991), although the biological significance of its kinase activity remains unknown. Similarly, 6-phosphofructo-2-kinase/fructose-2,6-bisphosphatase 4 (PFKFB4) phosphorylates and activates the oncogenic steroid receptor coactivator 3 (SRC-3) to drive breast cancer (Dasgupta et al., 2018). These enzymes, together with CAD and PFAS, demonstrate enzymatic activity to modify both small molecules (such as metabolites) and large proteins under physiological conditions, qualifying them as moonlighting enzymes (Huberts and van der Klei, 2010). Whether other GATs possess nonmetabolic activities via protein deamidation to regulate fundamental biological processes begs for further investigation.

Deamidation Shunts RelA from Mediating the Expression of Inflammatory Genes to that of Glycolytic Enzymes

NF- κ B-regulated gene expression underpins a diverse spectrum of biological processes such as inflammation, apoptosis, and tumorigenesis. RelA is the transcriptionally active subunit of the prototype p50-RelA dimer. Post-translational modifications, e.g., phosphorylation and acetylation, of RelA have been reported to choreograph the timing and intensity of expression of NF- κ B-responsive genes via recruitment of transcription coactivators or suppressors (Huang et al., 2010). For example, phosphorylation of serine 276 within the transactivation domain of RelA facilitates the interaction with CBP-p300 and subsequent activation of RelA-bound promoters (Zhong et al., 1998). On the other hand, phosphorylation of serine 536 of RelA in macrophages induces RelA degradation to terminate NF- κ B activation (Pradère et al., 2016). Our study describes an unprecedented function of deamidation in shunting expression of NF- κ B-dependent genes to that of glycolytic enzymes. Interestingly, RelA deamidation also downregulates the expression of components of mitochondrial oxidative phosphorylation. This is consistent with the report that NF- κ B activation is required to promote mitochondrial oxidative phosphorylation via regulated gene expression (Mauro et al., 2011). Previous structural analyses have provided no hints regarding how deamidation specifies the selectivity of promoters that RelA transactivates. Our biochemical analysis indicates that RelA-DD behaves similarly to wild-type RelA in binding to I κ B α and translocating into the nucleus in response to TNF- α , but

failed to associate with NF- κ B-responsive promoters. Gel shift analysis using the N-terminal DNA-binding domain of RelA demonstrated that deamidation had no effect on its ability to directly bind an NF- κ B consensus sequence (data not shown). These results suggest that RelA-DD either is not recruited to the promoter or is not tethered to the promoter after recruitment. The deamidated RelA-DD is severely impaired in its ability to interact with p50 compared to wild-type RelA, supporting the conclusion that deamidation abolishes the ability of RelA to interact with p50 and to activate NF- κ B-responsive inflammatory gene expression.

In S phase, when CAD is highly active, cells replicate their genome in preparation for cell division. Transcription imposes an inevitable threat to hinder DNA replication machinery, which can lead to DNA damage and genomic instability (García-Muse and Aguilera, 2016). Thus, active transcription is restricted only to genes essential for the cell cycle, such as cyclins, cyclin-dependent kinases, and DNA replication components (Fischer and Müller, 2017). CAD-mediated deamidation and abrogation of the expression of NF- κ B-dependent genes may ensure the shutdown of gene expression unnecessary for the cell cycle to prevent transcription-replication collision. Indeed, activated CAD resides in the nucleus (Sigoillot et al., 2005) and may deamidate nuclear RelA to prevent the expression of inflammatory genes.

How does deamidated RelA activate the expression of glycolytic enzymes? Transcription factors function as ensembles that contain additional coregulators and their responsive elements in the promoter. Cell cycle-dependent transcription factors may cooperate with deamidated RelA at the promoters of the glycolytic enzymes to enable RelA-mediated gene expression. E2F coactivators regulate the expression of genes crucial for the G1 to S transition and are implicated in RelA-mediated gene expression under various conditions (Ankers et al., 2016; Araki et al., 2008). Future experiments, determining whether cell cycle-dependent transcription factors such as E2F and Myc (Meyer and Penn, 2008) are involved in gene expression induced by deamidated RelA, will elucidate the mechanism of deamidation in specifying promoters of transcription.

Glycolysis Enabled by Deamidated RelA Is Crucial for Tumorigenesis

Aerobic glycolysis is crucial for normal cell proliferation and is a hallmark of highly proliferative cancerous cells (Hanahan and Weinberg, 2011). Stratifying a number of human cancer cell lines of the colorectum, breast, and lung for their CAD expression, RelA deamidation and expression of glycolytic enzymes identified nearly half of them with a signature gene expression pattern driven by deamidated RelA. Moreover, a number of RelA mutants that are frequently found in human tumors demonstrated reduced NF- κ B activation alongside increased RelA deamidation and aerobic glycolysis. These findings suggest that the gain of function in metabolic reprogramming of tumor-associated RelA mutants, although it impairs NF- κ B activation, is advantageous for cancer cell proliferation. Indeed, inhibitors of key glycolytic transporters or enzymes (e.g., GPI and PFK) potently suppress the growth of human cancer cell lines *ex vivo* and *in vivo* in concordance with their level of CAD-mediated RelA deamidation.

NF- κ B activation facilitates tumorigenesis via halting apoptosis of cancerous cells and maintaining smoldering inflammation of the tumor microenvironment (Zhang et al., 2017).

Here, we uncovered a cryptic function of RelA in promoting aerobic glycolysis, cancer cell proliferation, and tumorigenesis. CAD deamidates RelA to enable its alternate function in activating glycolytic enzyme expression and promoting aerobic glycolysis, thus coupling glycolysis to nucleotide synthesis. The upregulated glycolytic enzymes, such as Glut3, HK4, PFKF, PKLR, PDK3, and PC, translate into significantly elevated intracellular metabolites, particularly those of the lower portion, of the glycolytic pathway. The accumulation of these metabolites may facilitate flux into the serine-glycine synthesis pathway that provides one-carbon units for nucleotide synthesis (Vander Heiden et al., 2009). Indeed, the expression of RelA-DD, but not RelA-64A, up-regulates glycolytic serine synthesis by ~120%. The effect of the glycolytic serine synthesis is further accentuated by the report that the glycolytic serine synthesis is coupled to serine uptake from extracellular milieu to avoid one-carbon unit wasting (Pa-cold et al., 2016), implying that the net increase in intracellular serine may be amplified by elevated uptake rate. In addition to one-carbon unit, aerobic glycolysis also supplies reducing power in the form of NADH or NADPH vital for the synthesis of nucleotides, lipids, amino acids, and other cellular building blocks (Cantor and Sabatini, 2012). The glycolysis-branched pentose phosphate pathway (PPP) also generates NADPH, and multiple components of the PPP pathway were upregulated by deamidated RelA-DD. The elevated expression of PC and PDK is expected to funnel pyruvate to synthesize oxaloacetate and malate. The glycolytic malate synthesis likely facilitates the balance of reducing power and carbon intermediates between the cytosol and the mitochondrial compartment, an essential process for proliferating cells (LaNoue and Williamson, 1971; Locasale and Cantley, 2011). Thus, CAD-mediated RelA deamidation choreographs a metabolic program to promote nucleotide synthesis. In essence, CAD-mediated deamidation and downstream gene expression, empowered by deamidated RelA, are common features of cancer cells, unveiling a fundamental mechanism underlying tumor-associated aerobic glycolysis and suggesting alternative cancer therapies.

Limitations of Study

The limitation of this study is the reliance on cultured cells, and thus future work entailing genetically modified rodent models (e.g., RelA-DD knockin and CAD-inducible knockout) will be necessary to establish the *in vivo* physiological and pathological roles of CAD-mediated RelA deamidation. Likewise, *in vivo* studies with genetically engineered animal models of human cancer are needed to determine whether this pathway can be pharmacologically targeted to treat cancer. In addition to tumor cells, immune cells such as T cells and macrophages quickly engage a glycolytic metabolic program to enable immune activation when encountered with microbial antigens (Chang et al., 2013; Fox et al., 2005; O'Neill et al., 2016). Whether the CAD-mediated RelA deamidation contributes to these metabolic processes as well remains to be determined.

STAR★METHODS

RESOURCE AVAILABILITY

Lead Contact—Further information and requests for reagents should be directed and will be fulfilled by the Lead Contact, Pinghui Feng (pinghuif@usc.edu).

Materials availability—All unique/stable reagents generated in this study are available from the Lead Contact without restriction.

Data and Code Availability—The accession numbers for RNA-sequencing datasets reported in this paper are publicly available at the NCBI Gene Expression Omnibus database (<https://www.ncbi.nlm.nih.gov/geo>) under accession numbers GEO: GSE132868 and GSE132871.

EXPERIMENTAL MODEL AND SUBJECT DETAILS

Cell Culture—HEK293T, HCT116, SW480, HT29, *Rela*^{-/-} mouse embryonic fibroblasts (MEF) and hTERT immortalized human fibroblasts (BJ5) were cultured in Dulbecco's modified Eagle's medium (DMEM, Corning) supplemented with 10% heat-inactivated fetal bovine serum (FBS; HyClone), penicillin (100 U/mL) and streptomycin (100 µg/mL). THP-1, T47D, H1975 and DLD-1 cells were cultured in RPMI 1640 medium supplemented with 10% FBS and antibiotics. LoVo cells were cultured in F12K medium (ThermoFisher) supplemented with 10% FBS and antibiotics. All other cancer cell lines were cultured in their corresponding medium according to the ATCC recommendation.

Mice—Inbred and outbred male homozygous *Foxn1*^{mu} mice (6 weeks of age) were purchased from the Jackson Laboratory and were subjected to sterile animal housing. Mice of 7-week-old were used for all the tumor xenograft experiments. Mice were randomized into the different treatment and control groups equilibrated for body weight and age. Mice were fed with regular diet. All experiments were performed following approval by the IACUC committee of University of Southern California (protocol number: 11730). Mice were held in SPF conditions on an individually ventilated rack HEPA-filtered system, on a 12:12 light cycle, with average temperatures ranging from 70°F to 74°F. Direct bedding consists of either “Sani-Chips” (hardwood chips) or “Diamond Dry” paper processing by-product. Mice were fed with either Purina 5053 Pico Lab irradiated rodent diet or Purina 5525 Pico Lab high energy irradiated breeder diet, and with reverse osmosis water from an automatic watering source.

Microbes—Sendai virus (Cantell strain) was purchased from Charles River. *Salmonella Typhimurium* was a gift from Dr. Andrew Ouellette at University of Southern California.

Plasmids—Luciferase reporter plasmids for the NF-κB, IFN-β promoter, RelA and its truncated mutants, RIG-I-N, MAVS, IKKβ, TBK1 and RelA were described previously (Dong et al., 2010; Dong and Feng, 2011; Dong et al., 2012; He et al., 2015; Seth et al., 2005). The non-silencing (control) shRNA and shRNA for human glutamine amidotransferases (CAD, PFAS, CTPS1/2, GMPS, PPAT, GFPT1/2, ASNS, NADSYN1, CPS1) and human UMPS were purchased from Thermo Scientific. Mammalian expression plasmid (pcDNA5 with Flag-tag sequence) for CAD was generated by molecular cloning, based on its cDNA construct purchased from Addgene. All point mutants, including CAD-C252S, RelA-N64A, RelA-N64D, RelA-N64D/N139D and cancer-associated RelA mutations were generated by site-directed mutagenesis and confirmed by sequencing.

Lentiviral expression plasmids for RelA mutants were generated in the vectors of pCDH-CMV-EF1-PURO or pCDH-CMV-EF1-Hygro by molecular cloning.

METHOD DETAILS

Quantitative Real-time PCR (qRT-PCR)—Quantitative Real-time PCR was performed as previously described (Zhao et al., 2016). Cells were infected with the indicated shRNAs or synchronized to the indicated time point. Total RNA was extracted using TRIzol reagent (Invitrogen). Complementary cDNA was synthesized from total RNA using reverse transcriptase (Invitrogen). cDNA was diluted, and analyzed by qRT-PCR using SYBR Green Master Mix (Applied Biosystems) with Step-One PCR instrument (Applied Biosystems). Relative mRNA expression for each target gene was calculated by the 2^{-Ct} method using *β -actin* as an internal control. The sequences of qRT-PCR primers are listed in Table S1.

Lentivirus-Mediated Stable Cell Line Construction—Lentiviruses were produced as previously described (Dong and Feng, 2011; Feng et al., 2008). Briefly, HEK293T cells were transfected with the packaging plasmids VSV-G, DR8.9 and the pCDH lentiviral expression vector or lentiviral shRNA plasmids. At 48 h post transfection, the supernatant was harvested and filtered (and concentrated by ultracentrifugation if necessary). HEK293T cells, MEFs, THP-1, HCT116, LoVo or HFF cells were infected with the supernatant in the presence of polybrene (8 μ g/mL) with centrifugation at 1800 rpm for 50 min at 30°C. Cells were selected at 48 h post infection and maintained in 10% FBS DMEM supplemented with puromycin (1~2 μ g/mL) or hygromycin (200 μ g/mL).

To establish RelA-reconstituted HCT116 or SW480 cells, cells were infected with puromycin-resistant lentiviral shRNA targeting the 3' UTR of RelA mRNA and RelA depletion was validated by immunoblot. RelA-depleted cells were infected with hygromycin-resistant lentivirus containing wild-type RelA, RelA-DD or RelA-64A. Reconstituted cells were then selected and maintained with puromycin (1 μ g/mL) and hygromycin (200 μ g/mL).

To establish CAD-knockout and P50-knockout cell lines, HEK293T were transduced with lentivirus expressing sgRNA for P50 (pL-CRISPR.EFS.PAC-sgRNA-Targeting-P50, Table S1, Exon 6) or CAD (pL-CRISPR.EFS.PAC-sgRNA-Targeting-CAD, Table S1, Exon6) and selected with 1 μ g/mL puromycin in DMEM containing 10% FBS. Medium was supplemented with 10 μ g/mL Uridine post lentiviral infection for sgRNA targeting CAD. Single colonies were isolated and screened by immunoblotting with P50/CAD antibody. CAD knockout cell lines were kept culturing in the presence of 10 μ g/mL Uridine.

To establish CAD-Flag knockin cell line, HCT116 was transduced with lentivirus expressing sgRNA for CAD (pL-CRISPR.EFS.PAC-sgRNA-Targeting-CAD, Table S1, Exon 43), together with the transfection of a donor plasmid (pFETCh_Donor, EMM0021, Addgene) containing 5' - and 3' -homology arms with sgRNA NGG-mutation. Single colonies were then isolated and screened by immunoblotting with CAD and Flag antibody. The positive clone was cultured in regular DMEM containing 10% FBS.

Microbes Infection and Molecule Treatment—Sendai virus was used for infection at [100 HA/mL]. Infection lasted for 2 h for the cell synchronization and two-dimensional gel electrophoresis (2DGE), 6 h for qRT-PCR analyses, 16 h for ELISA assays and 24 h for dual-luciferase reporter assays. Salmonella Typhimurium (PhoPc) was used for infection at 30 CFU/cell for 12 h. Recombinant TNF- α was administered at 10 ng/mL for 30 min for co-immunoprecipitation assays and 2DGE, and 6 h for qRT-PCR analyses. Lipopolysaccharide was administered at 100 ng/mL for 30 min for 2DGE analysis, 6 h for qRT-PCR analyses and 16 h for ELISA assays.

Mouse Embryonic Fibroblasts Extraction—Mouse embryonic fibroblasts were extracted from the fetuses of RelA-DD knock-in C57BL/6 mice (made by Cyagen) at day 14 of gestation. Briefly, the head and liver were removed, and the embryo was washed with PBS, minced and digested with Trypsin (Corning). DMEM containing 10% FBS was subsequently added and cells were cultured and passaged for 3 generations before being used for experiments.

Dual-Luciferase Reporter Assay—HEK293T cells, seeded in 24-well plates (~50% cell density), were transfected with an IFN- β or NF- κ B reporter plasmid cocktail (50 ng of luciferase reporter plasmid and 5 ng of pRL Renilla luciferase control vector) and the expression plasmids (empty plasmid, one or multiple plasmids depending on the experiment) by calcium phosphate precipitation. Whole cell lysates at 30 h post-transfection were used to determine the activity of firefly luciferase and Renilla luciferase by a microplate reader (FLUOstar Omega). When Sendai virus (SeV) was used, cells were infected with SeV [100 HA/mL] at 24 h post-transfection and whole cell lysates were harvested at 48 h.

Protein Expression and Purification—HEK293T cells were transfected with the expression vector containing Flag-tagged genes of interest for 48 h. Cells were harvested and lysed with Triton X-100 buffer (20 mM Tris, pH 7.5, 150 mM NaCl, 1.5 mM MgCl₂, 20 mM β -glycerophosphate, 1 mM sodium orthovanadate, 10% glycerol, 0.5 mM EGTA, 0.5% Triton X-100) supplemented with a protease inhibitor cocktail (Roche). Whole cell lysates were sonicated and centrifuged at 12,000 rpm for 15 min. Supernatant was harvested, filtered, pre-cleared with protein A/G agarose beads at 4°C for 1 h and then incubated with anti-Flag agarose beads at 4°C for 4 h. The agarose beads were washed extensively and eluted with 0.2 mg/mL 3xFlag peptide. The purity of the eluted proteins was analyzed by SDS gel electrophoresis and silver staining.

Co-immunoprecipitation (Co-IP) and Immunoblotting—For Co-IP using exogenous protein, HEK293T cells were transfected with indicated expression plasmids for 48 h. For Co-IP using endogenous proteins, cells were directly harvested for experiments. Whole cell lysates were prepared with NP40 buffer (50 mM Tris-HCl, pH 7.4, 150 mM NaCl, 1% NP-40, 5 mM EDTA) supplemented with 20 mM β -glycerophosphate and 1 mM sodium orthovanadate. Whole cell lysates were sonicated, centrifuged and pre-cleared with protein A/G agarose for 1 h. Pre-cleared samples were then incubated with indicated antibodies overnight and protein A/G agarose for 1 h at 4°C, or with antibody/glutathione-conjugated agarose for 4 h at 4°C. The agarose beads were washed extensively, and samples were eluted

by boiling at 95°C for 10 min. Precipitated proteins were analyzed by SDS gel electrophoresis and immunoblotting.

All immunoblotting was performed using the indicated primary antibodies (1:1000 dilution) and IRDye800-conjugated secondary antibodies (1:10,000 dilution, Li-Cor). Proteins were visualized by Odyssey infrared imaging system (Li-Cor).

Oxygen Consumption Rate and Extracellular Acidification Rate—Approximately 1.5×10^5 of HCT116 stable cells were seeded on a poly-D-lysine coated XF24 plate. Oxygen consumption rate (OCR) was measured using the mitochondrial stress test kit in Seahorse XF Base Medium media (10 mM glucose, 2 mM L-glutamine, and 1 mM sodium pyruvate) under basal conditions (ECAR) and in response to 1.0 μ M oligomycin, 0.5 μ M fluoro-carbonyl cyanide phenylhydrazone (FCCP) and 0.5 μ M rotenone/antimycin A with the XF24 Extracellular Flux Analyzer (Agilent).

Approximately 3×10^4 of HCT116 stable cells were seeded on a poly-D-lysine coated XF96 plate. Extracellular acidification rate (ECAR) was measured using the glycolysis stress test kit in Seahorse XF Base Medium media (10 mM glucose, 2 mM L-glutamine, and 1 mM sodium pyruvate) in response to 20 mM glucose, 1 μ M oligomycin and 50 mM 2-Deoxyglucose with the XF96 Extracellular Flux Analyzer (Agilent).

Cell Proliferation Assay—The *in vitro* cell viability test was performed with Cell Proliferation Kit II (XTT) according to the manufacturer's recommendation (Sigma). Briefly, cells were seeded at a density of 1×10^4 cells per well in 96-well culture plates. After 15 h, the medium was replaced with one that contains increasing concentrations of 2-deoxyglucose (2-DG, Sigma) or PFK158 (SelleckChem) and cells were cultured for 24 h. XTT was then added to the medium and cell viability in each well was measured by absorption at a wavelength of 475 nm, with 660 nm as the reference wavelength. Each data point was performed in triplicate. Cell viability was presented as the percentage of absorption at a given concentration of inhibitors divided by the maximum absorption at zero concentration.

RNA Library Preparation and Sequencing—RNA sequencing libraries were prepared using the KAPA RNA-Seq library preparation kit (KAPA Biosystems, Roche) for mRNA sequencing according to the manufacturer's protocol. RNA sequencing was performed on Illumina NextSeq 500 at the USC Molecular Genomics Core.

RNA sequencing results were processed using the new Tuxedo protocol. Reads were aligned to the hg38 genome or mm10 using HISAT (v2.1.0)(Kim et al., 2015). Transcripts were assembled and quantified using StringTie (v1.3.6)(Pertea et al., 2016). Differential gene expression was analyzed using DESeq2 (v1.16.1)(Love et al., 2014), genes were annotated using KEGG(Kanehisa et al., 2016) and GO(Mi et al., 2017) database, and annotated genes were subjected to clusterProfiler(Yu et al., 2012) for pathway enrichment analysis.

Sequencing data are available at: <https://www.ncbi.nlm.nih.gov/geo/> with the ID number GSE132868 and GSE132871.

Lactate Colorimetric Assay—Cancer cells (2×10^5) were seeded in 12-well for 14 h. The medium was harvested and filtered by a 10kD MW spin filter (Thermo) and lactate was measured by the Lactate Assay Kit (Sigma) according to the manufacturer's protocol. Tumor samples were homogenized in lactate assay followed by filtering according to the manufacturer's protocol.

Cell Synchronization

1. S phase Synchronization: HCT116/BJ5 cells were seeded at 20% confluency and then synchronized by double thymidine block method as previously described (Chen and Deng, 2018). Briefly, cells were cultured in their corresponding medium containing 2 mM thymidine for 15 h then replaced with fresh medium for 10 h, followed by a second thymidine block (2 mM) to synchronize cells at the S phase checkpoint. Upon releasing by replacement of fresh medium, cells were harvested at multiple time points for western blotting, two-dimensional gel electrophoresis and real-time PCR analysis on indicated proteins/genes.
2. G0/G1 phase Synchronization: HCT116/BJ5 cells were seeded at 40% confluency and then synchronized by lovastatin method as previously described (Javanmoghadam-Kamrani and Keyomarsi, 2008). Briefly, cells were arrested in G0/G1 phase by incubation with medium containing lovastatin (10 μ M) for 15 h. Upon releasing by replacing medium containing 100-fold excess of mevalonate, cells were harvested at multiple time points for western blotting, two-dimensional gel electrophoresis and real-time PCR analysis on indicated proteins/genes.

Metabolic Profiling and Isotope Tracing—Reconstituted HCT116 cells (2×10^7) per sample (in triplicates) were harvested for metabolomics analysis performed by Metabolon Inc.

Isotope tracing experiments were performed as previously described (Delfarah et al., 2019; Jang et al., 2018; Sauer, 2006). For glycolytic rate analysis, 'reconstituted' HCT116 cells were cultured with medium containing [U- 13 C]-labeled glucose (Cambridge Isotope Laboratories) for 15 min. For Pyruvate Carboxylase (PC) activity, 'reconstituted' HCT116 cells were cultured with medium containing [1- 13 C]-pyruvate for 30 min. Metabolite extraction was performed upon labeling. For extraction of intracellular metabolites, cells were washed on ice with 1 mL ice-cold 150 mM ammonium acetate (NH_4AcO , pH 7.3). 1 mL of -80°C cold 80% MeOH was added to the wells, samples were incubated at -80°C for 20 min, then cells were scraped off and supernatants were transferred into microfuge tubes. Samples were pelleted at 4°C for 5 min at 15k rpm. The supernatants were transferred into microfuge tube, the cell pellets were re-extracted with 200 μ l ice-cold 80% MeOH, spun down and the supernatants were combined. Metabolites were dried at room temperature under vacuum and re-suspended in water for LC-MS run.

Samples were randomized and analyzed on a Q Exactive Plus hybrid quadrupole-Orbitrap mass spectrometer coupled to an UltiMate 3000 UHPLC system (Thermo Scientific). The mass spectrometer was run in polarity switching mode ($+3.00$ kV/ -2.25 kV) with an m/z

window ranging from 65 to 975. Mobile phase A was 5 mMNH₄AcO, pH 9.9, and mobile phase B was acetonitrile. Metabolites were separated on a Luna 3 μm NH₂ 100Å (150 × 2.0 mm) column (Phenomenex). The flowrate was 300 μl/min, and the gradient was from 15% A to 95% A in 18 min, followed by an isocratic step for 9 min and re-equilibration for 7 min. All samples were run in biological triplicate.

Metabolites were detected and quantified as area under the curve based on retention time and accurate mass (± 5 ppm) using the TraceFinder 3.3 (Thermo Scientific) software. Raw data was corrected for naturally occurring ¹³C abundance (Moseley, 2010).

Two-dimensional Gel Electrophoresis—Cells (1 × 10⁶) were lysed in 150 μl rehydration buffer (8 M Urea, 2% CHAPS, 0.5% IPG Buffer, 0.002% bromophenol blue) by three pulses of sonication and whole cell lysates were centrifuged at 20,000 g for 15 min. Supernatants were loaded to IEF strips for focusing with a program comprising: 20 V, 10 h (rehydration); 500 V, 1 h; 1000 V, 1 h; 1000–5000 V, 4 h; 5000 V, 4 h. After IEF, strips were incubated with SDS equilibration buffer (50 mM Tris-HCl [pH8.8], 6 M urea, 30% glycerol, 2% SDS, 0.001% Bromophenol Blue) containing 10 mg/mL DTT for 15 min and then SDS equilibration buffer containing 2-iodoacetamide for 15 min. Strips were washed with SDS-PAGE buffer, resolved by SDS-PAGE, and analyzed by immunoblotting.

In Vitro Deamidation Assay—GST-RelA, CAD and CAD-C/S mutant were purified from transfected 293T cells to homogeneity as determined by silver staining. *In vitro* on-column deamidation of RelA was performed as previously reported (He et al., 2015; Zhao et al., 2016). Briefly, ~0.2 μg of CAD or CAD C/S, and 0.6 μg of GST-RelA (bound to glutathione-conjugated agarose) were added to a total volume of 30 μl. The reaction was carried out at 30°C for 45 min in deamidation buffer (100 mM Tris-HCl at pH 8.0, 100 mM KCl, 1 mM dithiothreitol, 20.2 mM aspartate, 1.5 mM ATP, 200 mM phosphoribosyl 5'-pyrophosphate, 3.5 mM MgCl₂, and 5 mM NaHCO₃). Protein-bound GST beads were washed with deamidation buffer and GST-RelA was eluted with rehydration buffer (8 M Urea, 2% CHAPS, 0.5% IPG Buffer, 0.002% bromophenol blue) at room temperature. Samples were then analyzed by two-dimensional gel electrophoresis and immunoblotting.

Xenograft Nude Mouse Model—A total of 1 × 10⁶ 'reconstituted' HCT116 cells or 2 × 10⁶ LoVo stably expressing RelA mutant cells (in log phase growth) in 100 μL PBS were injected subcutaneously in the dorsal flank of the mice (n = 5). Tumor size were measured with calipers three times a week. The tumor volume was calculated using the equation: Volume = (length × width²)/2. Tumors were harvested and weighed at Day 35 for the reconstituted HCT116 cells and Day 40 for the LoVo stable cells.

A total of 1 × 10⁶ HT29, HCT116 or LoVo cells (in log phase growth) in 100 μL PBS were injected subcutaneously in the dorsal flank of the mice (n = 12). Once adequate tumor volumes became established (minimum 100 mm³), the animals were randomized and divided into two groups. One group received intraperitoneal PFK158 (SelleckChem, 25 mg/kg body weight in 5% DMSO, 45% PEG300, 1% Tween80, once every three days for a total of 6 injections) and the other group was injected with buffer. Body weight and tumor

size were measured with calipers every day. Tumors were harvested and weighed at Day 18 post treatment.

Mass Spectrometry Analysis—For identification of deamidation sites, HEK293T/Flag-RelA stable cell line was transfected with an expression plasmid containing CAD or CAD-C/S (deamidase-dead) mutant. Flag-RelA was purified by anti-Flag-conjugated agarose beads for 4 h at 4°C. Beads were then extensively washed and RelA was eluted with 3xFlag peptide at 0.2 mg/mL. Purified RelA was subjected to SDS-PAGE electrophoresis and gel slices were prepared for in-gel digestion and Mass Spectrometry analysis (USC Mass Spectrometry Core Facility).

Propidium Iodide Staining—Reconstituted HCT116 cells (2×10^5) were harvested and washed in PBS. Cells were then fixed in 70% Ethanol for 30 min at 4°C, washed with PBS and treated with 50 μ L of PBS containing RNase (100 μ g/mL). A volume of 200 μ L PBS containing propidium iodide (50 μ g/mL, Sigma) was then added to the solution. Cells were analyzed by FACSCalibur (BD Biosciences) and 10,000 events were collected per sample. Data was analyzed by FlowJo.

Data Mining with cBioPortal—All data mining was performed using cBioPortal (Cerami et al., 2012; Gao et al., 2013). The study database includes Cancer Cell Line Encyclopedia (novartis/broad, Nature 2012), Colorectal Adenocarcinoma (TCGA and Genentech, Nature 2012), Breast Invasive Carcinoma (TCGA, Nature, 2012), Brain Lower Grade Glioma (TCGA, PanCancer Atlas), Stomach Adenocarcinoma (TCGA, PanCancer Atlas), Kidney Renal Clear Cell Carcinoma (BGI, Nature Genetics), Kidney Renal Clear Cell Carcinoma (TCGA, Nature, 2013), Small Cell Lung Cancer (CLCGP, Nat Genet 2012), Small Cell Lung Cancer (Johns Hopkins, Nat Genet 2012), Lung Adenocarcinoma (Broad, Cell 2012), Lung Squamous Cell Carcinoma (TCGA, Nature 2012), Ovarian Serous Cystadenocarcinoma (TCGA, Provisional), Skin Cutaneous Melanoma (TCGA, Provisional) and Uterine Corpus Endometrial Carcinoma (TCGA, Nature 2013). RelA mutations were selected based on their risk impact factor (Medium and High). All searches were performed according to the cBioPortal's online instructions.

QUANTIFICATION AND STATISTICAL ANALYSIS

Data are presented as mean \pm standard deviation (SD), if not stated in the figure legend. Statistical analyses were performed by un-paired, two-tailed Student's t test (unless specified). For more than two groups data were analyzed by ANOVA followed by the un-paired Student's t test. Statistical analyses were performed with Excel or Graphpad Prism. A p value less than 0.05 is considered statistically significant. *, $p < 0.05$; **, $p < 0.01$; ***, $p < 0.001$. No statistical methods were used to estimate sample size. All samples were included in the analyses.

Supplementary Material

Refer to Web version on PubMed Central for supplementary material.

ACKNOWLEDGMENTS

We thank Drs. Chengyu Liang, Min Yu, and Ite Offringa for human cancer cell lines, Lin-Feng Chen for *Rela*^{-/-} MEFs, Jiang-Jian Hao for mass spectrometry analysis, Andrew Ouellette for *Salmonella Typhimurium*, and Bridget Samuel for proof-reading our manuscript. This work was supported by grants from NIDCR (DE028973 to J.Z., DE027556 and DE026003 to P.F.) and NCI (CA221521 to P.F.), startup funds from the Herman Ostrow School of Dentistry of USC (P.F.) and CAMS (CAMS-I2M and 2016-I2M-1-005 to T.J.), and grants from National Natural Science Foundation of China (31671371 to T.J.) and Central Public Interest Scientific Institution of Basal Research (2016ZX310195, 2017PT31026, and 2018PT31016 to T.J.).

REFERENCES

- Adams V, Griffin LD, Gelb BD, and McCabe ER (1991). Protein kinase activity of rat brain hexokinase. *Biochem. Biophys. Res. Commun* 177, 1101–1106. [PubMed: 2059200]
- Ankers JM, Awais R, Jones NA, Boyd J, Ryan S, Adamson AD, Harper CV, Bridge L, Spiller DG, Jackson DA, et al. (2016). Dynamic NF- κ B and E2F interactions control the priority and timing of inflammatory signalling and cell proliferation. *eLife* 5, 10.7554/eLife.10473.27185527.
- Araki K, Kawachi K, and Tanaka N (2008). IKK/NF-kappaB signaling pathway inhibits cell-cycle progression by a novel Rb-independent suppression system for E2F transcription factors. *Oncogene* 27, 5696–5705. [PubMed: 18542057]
- Ben-Sahra I, Howell JJ, Asara JM, and Manning BD (2013). Stimulation of de novo pyrimidine synthesis by growth signaling through mTOR and S6K1. *Science* 339, 1323–1328. [PubMed: 23429703]
- Cantor JR, and Sabatini DM (2012). Cancer cell metabolism: one hallmark, many faces. *Cancer Discov* 2, 881–898. [PubMed: 23009760]
- Cerami E, Gao J, Dogrusoz U, Gross BE, Sumer SO, Aksoy BA, Jacobsen A, Byrne CJ, Heuer ML, Larsson E, et al. (2012). The cBio cancer genomics portal: an open platform for exploring multidimensional cancer genomics data. *Cancer Discov* 2, 401–404. [PubMed: 22588877]
- Chang CH, Curtis JD, Maggi LB Jr., Faubert B, Villarino AV, O’Sullivan D, Huang SC, van der Windt GJ, Blagih J, Qiu J, et al. (2013). Posttranscriptional control of T cell effector function by aerobic glycolysis. *Cell* 153, 1239–1251. [PubMed: 23746840]
- Chen G, and Deng X (2018). Cell Synchronization by Double Thymidine Block. *Bio. Protoc* 8, 10.21769/BioProtoc.2994.
- Chen YQ, Ghosh S, and Ghosh G (1998). A novel DNA recognition mode by the NF-kappa B p65 homodimer. *Nat. Struct. Biol* 5, 67–73. [PubMed: 9437432]
- Clem BF, O’Neal J, Tapolsky G, Clem AL, Imbert-Fernandez Y, Kerr DA 2nd, Klarer AC, Redman R, Miller DM, Trent JO, et al. (2013). Targeting 6-phosphofructo-2-kinase (PFKFB3) as a therapeutic strategy against cancer. *Mol. Cancer Ther* 12, 1461–1470. [PubMed: 23674815]
- Dasgupta S, Rajapakshe K, Zhu B, Nikolai BC, Yi P, Putluri N, Choi JM, Jung SY, Coarfa C, Westbrook TF, et al. (2018). Metabolic enzyme PFKFB4 activates transcriptional coactivator SRC-3 to drive breast cancer. *Nature* 556, 249–254. [PubMed: 29615789]
- Delfarah A, Parrish S, Junge JA, Yang J, Seo F, Li S, Mac J, Wang P, Fraser SE, and Graham NA (2019). Inhibition of nucleotide synthesis promotes replicative senescence of human mammary epithelial cells. *J. Biol. Chem* 294, 10564–10578. [PubMed: 31138644]
- Dong X, and Feng P (2011). Murine gamma herpesvirus 68 hijacks MAVS and IKK β to abrogate NF κ B activation and antiviral cytokine production. *PLoS Pathog* 7, e1002336. [PubMed: 22110409]
- Dong X, Feng H, Sun Q, Li H, Wu TT, Sun R, Tibbetts SA, Chen ZJ, and Feng P (2010). Murine gamma-herpesvirus 68 hijacks MAVS and IKKbeta to initiate lytic replication. *PLoS Pathog* 6, e1001001. [PubMed: 20686657]
- Dong X, He Z, Durakoglugil D, Arneson L, Shen Y, and Feng P (2012). Murine gammaherpesvirus 68 evades host cytokine production via replication transactivator-induced RelA degradation. *J. Virol* 86, 1930–1941. [PubMed: 22130545]

- Feng H, Dong X, Negaard A, and Feng P (2008). Kaposi's sarcoma-associated herpesvirus K7 induces viral G protein-coupled receptor degradation and reduces its tumorigenicity. *PLoS Pathog* 4, e1000157. [PubMed: 18802460]
- Fischer M, and Müller GA (2017). Cell cycle transcription control: DREAM/MuvB and RB-E2F complexes. *Crit. Rev. Biochem. Mol. Biol* 52, 638–662. [PubMed: 28799433]
- Fox CJ, Hammerman PS, and Thompson CB (2005). Fuel feeds function: energy metabolism and the T-cell response. *Nat. Rev. Immunol* 5, 844–852. [PubMed: 16239903]
- Gao J, Aksoy BA, Dogrusoz U, Dresdner G, Gross B, Sumer SO, Sun Y, Jacobsen A, Sinha R, Larsson E, et al. (2013). Integrative analysis of complex cancer genomics and clinical profiles using the cBioPortal. *Sci. Signal* 6, pl1. [PubMed: 23550210]
- García-Muse T, and Aguilera A (2016). Transcription-replication conflicts: how they occur and how they are resolved. *Nat. Rev. Mol. Cell Biol* 17, 553–563. [PubMed: 27435505]
- Graves LM, Guy HI, Kozlowski P, Huang M, Lazarowski E, Pope RM, Collins MA, Dahlstrand EN, Earp HS 3rd, and Evans DR (2000). Regulation of carbamoyl phosphate synthetase by MAP kinase. *Nature* 403, 328–332. [PubMed: 10659854]
- Hanahan D, and Weinberg RA (2011). Hallmarks of cancer: the next generation. *Cell* 144, 646–674. [PubMed: 21376230]
- He S, Zhao J, Song S, He X, Minassian A, Zhou Y, Zhang J, Brulois K, Wang Y, Cabo J, et al. (2015). Viral pseudo-enzymes activate RIG-I via deamidation to evade cytokine production. *Mol. Cell* 58, 134–146. [PubMed: 25752576]
- He CL, Bian YY, Xue Y, Liu ZX, Zhou KQ, Yao CF, Lin Y, Zou HF, Luo FX, Qu YY, et al. (2016). Pyruvate Kinase M2 Activates mTORC1 by Phosphorylating AKT1S1. *Sci. Rep* 6, 21524. [PubMed: 26876154]
- Huang B, Yang XD, Lamb A, and Chen LF (2010). Posttranslational modifications of NF-kappaB: another layer of regulation for NF-kappaB signaling pathway. *Cell. Signal* 22, 1282–1290. [PubMed: 20363318]
- Huberts DH, and van der Klei IJ (2010). Moonlighting proteins: an intriguing mode of multitasking. *Biochim. Biophys. Acta* 1803, 520–525. [PubMed: 20144902]
- Jang C, Chen L, and Rabinowitz JD (2018). Metabolomics and Isotope Tracing. *Cell* 173, 822–837. [PubMed: 29727671]
- Javanmoghdam-Kamrani S, and Keyomarsi K (2008). Synchronization of the cell cycle using lovastatin. *Cell Cycle* 7, 2434–2440. [PubMed: 18677105]
- Kanehisa M, Sato Y, Kawashima M, Furumichi M, and Tanabe M (2016). KEGG as a reference resource for gene and protein annotation. *Nucleic Acids Res* 44 (D1), D457–D462. [PubMed: 26476454]
- Kim D, Langmead B, and Salzberg SL (2015). HISAT: a fast spliced aligner with low memory requirements. *Nat. Methods* 12, 357–360. [PubMed: 25751142]
- LaNoue KF, and Williamson JR (1971). Interrelationships between malate-aspartate shuttle and citric acid cycle in rat heart mitochondria. *Metabolism* 20, 119–140. [PubMed: 4322086]
- Li J, Zhao J, Xu S, Zhang S, Zhang J, Xiao J, Gao R, Tian M, Zeng Y, Lee K, et al. (2019). Antiviral activity of a purine synthesis enzyme reveals a key role of deamidation in regulating protein nuclear import. *Sci. Adv* 5, eaaw7373. [PubMed: 31633017]
- Locasale JW, and Cantley LC (2011). Metabolic flux and the regulation of mammalian cell growth. *Cell Metab* 14, 443–451. [PubMed: 21982705]
- Love MI, Huber W, and Anders S (2014). Moderated estimation of fold change and dispersion for RNA-seq data with DESeq2. *Genome Biol* 15, 550. [PubMed: 25516281]
- Massière F, and Badet-Denisot MA (1998). The mechanism of glutamine-dependent amidotransferases. *Cell. Mol. Life Sci* 54, 205–222. [PubMed: 9575335]
- Mauro C, Leow SC, Anso E, Rocha S, Thotakura AK, Tornatore L, Moretti M, De Smaele E, Beg AA, Tergaonkar V, et al. (2011). NF- κ B controls energy homeostasis and metabolic adaptation by upregulating mitochondrial respiration. *Nat. Cell Biol* 13, 1272–1279. [PubMed: 21968997]
- Metallo CM, Gameiro PA, Bell EL, Mattaini KR, Yang J, Hiller K, Jewell CM, Johnson ZR, Irvine DJ, Guarente L, et al. (2011). Reductive glutamine metabolism by IDH1 mediates lipogenesis under hypoxia. *Nature* 481, 380–384. [PubMed: 22101433]

- Meyer N, and Penn LZ (2008). Reflecting on 25 years with MYC. *Nat. Rev. Cancer* 8, 976–990. [PubMed: 19029958]
- Mi H, Huang X, Muruganujan A, Tang H, Mills C, Kang D, and Thomas PD (2017). PANTHER version 11: expanded annotation data from Gene Ontology and Reactome pathways, and data analysis tool enhancements. *Nucleic Acids Res* 45 (D1), D183–D189. [PubMed: 27899595]
- Mogilenko DA, Haas JT, L’homme L, Fleury S, Quemener S, Levavasseur M, Becquart C, Wartelle J, Bogomolova A, Pineau L, et al. (2019). Metabolic and Innate Immune Cues Merge into a Specific Inflammatory Response via the UPR. *Cell* 178, 263. [PubMed: 31251916]
- Moseley HN (2010). Correcting for the effects of natural abundance in stable isotope resolved metabolomics experiments involving ultra-high resolution mass spectrometry. *BMC Bioinformatics* 11, 139. [PubMed: 20236542]
- Nolan GP, Ghosh S, Liou HC, Tempst P, and Baltimore D (1991). DNA binding and I kappa B inhibition of the cloned p65 subunit of NF-kappa B, a rel-related polypeptide. *Cell* 64, 961–969. [PubMed: 2001591]
- O’Neill LA, Kishton RJ, and Rathmell J (2016). A guide to immunometabolism for immunologists. *Nat. Rev. Immunol* 16, 553–565. [PubMed: 27396447]
- Pacold ME, Brimacombe KR, Chan SH, Rohde JM, Lewis CA, Swier LJ, Possemato R, Chen WW, Sullivan LB, Fiske BP, et al. (2016). A PHGDH inhibitor reveals coordination of serine synthesis and one-carbon unit fate. *Nat. Chem. Biol* 12, 452–458. [PubMed: 27110680]
- Perkins ND (2004). NF-kappaB: tumor promoter or suppressor? *Trends Cell Biol* 14, 64–69. [PubMed: 15102437]
- Pertea M, Kim D, Pertea GM, Leek JT, and Salzberg SL (2016). Transcript-level expression analysis of RNA-seq experiments with HISAT, StringTie and Ballgown. *Nat. Protoc* 11, 1650–1667. [PubMed: 27560171]
- Phelps CB, Sengchanthalangsy LL, Malek S, and Ghosh G (2000). Mechanism of kappa B DNA binding by Rel/NF-kappa B dimers. *J. Biol. Chem* 275, 24392–24399. [PubMed: 10825175]
- Pradère JP, Hernandez C, Koppe C, Friedman RA, Luedde T, and Schwabe RF (2016). Negative regulation of NF- κ B p65 activity by serine 536 phosphorylation. *Sci. Signal* 9, ra85. [PubMed: 27555662]
- Robitaille AM, Christen S, Shimobayashi M, Cornu M, Fava LL, Moes S, Prescianotto-Baschong C, Sauer U, Jenoe P, and Hall MN (2013). Quantitative phosphoproteomics reveal mTORC1 activates de novo pyrimidine synthesis. *Science* 339, 1320–1323. [PubMed: 23429704]
- Sauer U (2006). Metabolic networks in motion: ¹³C-based flux analysis. *Mol. Syst. Biol* 2, 62. [PubMed: 17102807]
- Sen R, and Baltimore D (1986). Multiple nuclear factors interact with the immunoglobulin enhancer sequences. *Cell* 46, 705–716. [PubMed: 3091258]
- Seth RB, Sun L, Ea CK, and Chen ZJ (2005). Identification and characterization of MAVS, a mitochondrial antiviral signaling protein that activates NF-kappaB and IRF 3. *Cell* 122, 669–682. [PubMed: 16125763]
- Seth RB, Sun L, and Chen ZJ (2006). Antiviral innate immunity pathways. *Cell Res* 16, 141–147. [PubMed: 16474426]
- Shoaf WT, and Jones ME (1973). Uridylic acid synthesis in Ehrlich ascites carcinoma. Properties, subcellular distribution, and nature of enzyme complexes of the six biosynthetic enzymes. *Biochemistry* 12, 4039–4051. [PubMed: 4355548]
- Sigoillot FD, Berkowski JA, Sigoillot SM, Kotsis DH, and Guy HI (2003). Cell cycle-dependent regulation of pyrimidine biosynthesis. *J. Biol. Chem* 278, 3403–3409. [PubMed: 12438317]
- Sigoillot FD, Kotsis DH, Serre V, Sigoillot SM, Evans DR, and Guy HI (2005). Nuclear localization and mitogen-activated protein kinase phosphorylation of the multifunctional protein CAD. *J. Biol. Chem* 280, 25611–25620. [PubMed: 15890648]
- Takeuchi O, and Akira S (2010). Pattern recognition receptors and inflammation. *Cell* 140, 805–820. [PubMed: 20303872]
- Vander Heiden MG, Cantley LC, and Thompson CB (2009). Understanding the Warburg effect: the metabolic requirements of cell proliferation. *Science* 324, 1029–1033. [PubMed: 19460998]

- Yang W, Xia Y, Hawke D, Li X, Liang J, Xing D, Aldape K, Hunter T, Alfred Yung WK, and Lu Z (2012). PKM2 phosphorylates histone H3 and promotes gene transcription and tumorigenesis. *Cell* 150, 685–696. [PubMed: 22901803]
- Yu G, Wang LG, Han Y, and He QY (2012). clusterProfiler: an R package for comparing biological themes among gene clusters. *OMICS* 16, 284–287. [PubMed: 22455463]
- Zhang Q, Lenardo MJ, and Baltimore D (2017). 30 Years of NF- κ B: A Blossoming of Relevance to Human Pathobiology. *Cell* 168, 37–57. [PubMed: 28086098]
- Zhao J, Zeng Y, Xu S, Chen J, Shen G, Yu C, Knipe D, Yuan W, Peng J, Xu W, et al. (2016). A Viral Deamidase Targets the Helicase Domain of RIG-I to Block RNA-Induced Activation. *Cell Host Microbe* 20, 770–784. [PubMed: 27866900]
- Zhong H, Voll RE, and Ghosh S (1998). Phosphorylation of NF-kappa B p65 by PKA stimulates transcriptional activity by promoting a novel bivalent interaction with the coactivator CBP/p300. *Mol. Cell* 1, 661–671. [PubMed: 9660950]

Highlights

- CAD, the rate-limiting *de novo* pyrimidine synthesis enzyme, deamidates RelA
- Deamidation shunts RelA from mediating an inflammatory response to aerobic glycolysis
- Deamidation of RelA occurs in a cell cycle-dependent manner
- Cancer cells hijack RelA deamidation to promote glycolysis and tumorigenesis

Context and Significance

Cell proliferation and inflammatory response are two metabolically competing biological processes in non-immune cells. For instance, highly proliferating cells produce lower levels of inflammatory cytokines than nonproliferating cells. How cell proliferation attenuates inflammatory response remains unclear. Here, Zhao and colleagues show that the enzyme carbamoyl-phosphate synthetase, aspartate transcarbamoylase, and dihydroorotase (CAD) deamidates RelA, a subunit of the pro-inflammatory mediator NF- κ B, to shunt the cell's gene expression from those encoding inflammatory mediators to glycolytic enzymes. They also found that various cancer cell lines hijack CAD-mediated RelA deamidation via high CAD expression and/or RelA mutations to promote glycolysis and thus tumor proliferation. These data suggest that glycolysis driven by CAD-mediated RelA deamidation can potentially guide the stratification and treatment of diverse human cancers.

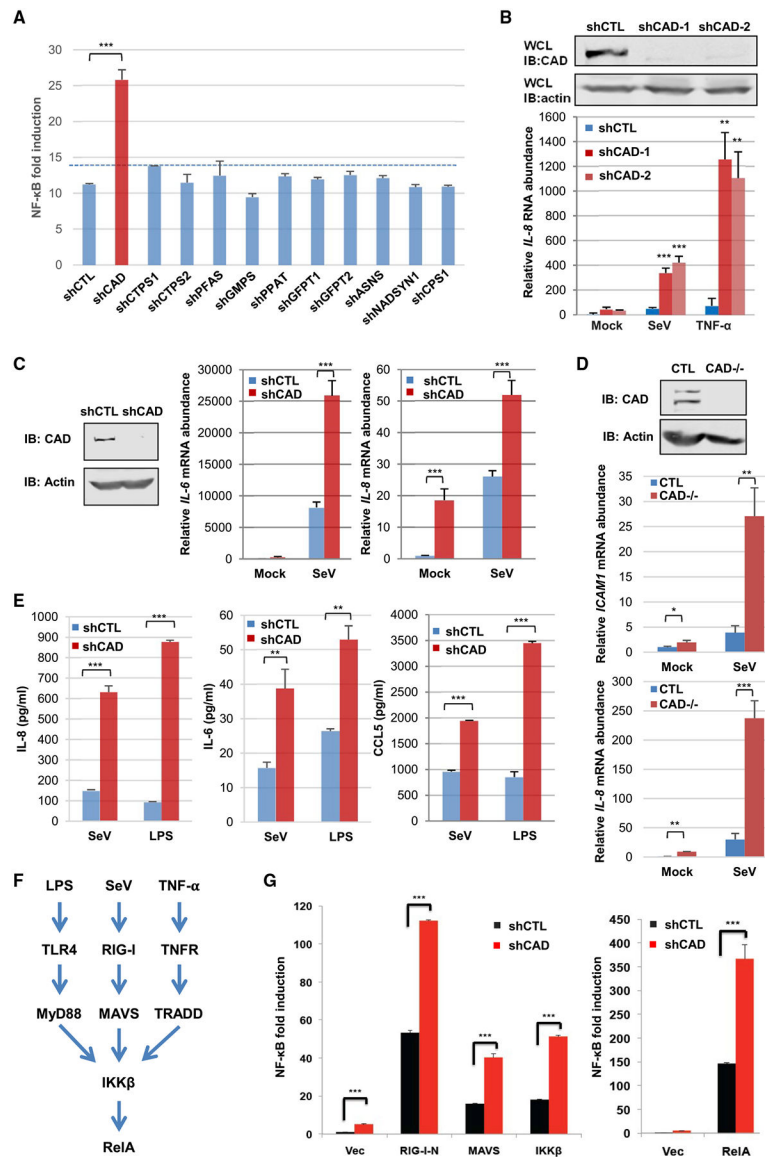


Figure 1. CAD Negatively Regulates NF-κB Activation

(A) NF-κB luciferase reporter assay from 293T cells with shRNA targeting indicated cellular glutamine amidotransferases upon Sendai virus (SeV) infection. CTPS: CTP synthetase; PFAS: phosphoribosylformylglycinamide synthetase; GMPS: GMP synthetase; GFPT: glutamine fructose-6-phosphate amidotransferase; ASNS: Asparagine synthetase; NADSYN1: NAD synthetase 1; CPS1: carbamoyl-phosphate synthetase; and PPAT: phosphoribosyl pyrophosphate amidotransferase. CAD, please see text.

(B) Immunoblots of CAD from whole cell lysates (WCLs) of 293T cells depleted for CAD by two different shRNAs (shCAD-1 and shCAD-2) versus a control shRNA (shCTL) (top) and *IL-8* abundance in 293T cells depleted for CAD and after infection with SeV or treatment with TNF-α (bottom).

(C) Immunoblots of CAD from WCLs of human THP-1 monocytes (left panels) and *IL-6* or *IL-8* abundance in control (shCTL) or CAD-depleted (shCAD) THP-1 cells after SeV infection.

(D) Immunoblots of CAD from WCLs of CTL and CAD-knockout 293T cells (top panels) and *ICAM1* or *IL-8* abundance in CTL and CAD-knockout 293T cells infected with SeV (bottom panels).

(E) IL-8, IL-6, and CCL5 concentration from THP-1 monocytes treated with SeV or lipopolysaccharide (LPS).

(F) Diagram of the NF- κ B pathway that can be triggered by distinct stimuli, which converge at the IKK kinase complex.

(G) NF- κ B luciferase reporter assay from 293T cells transfected with indicated components of the RIG-I-RelA pathway.

Data are presented as mean \pm SD. Significance was calculated using two-tailed, unpaired Student's t test. **p < 0.01; ***p < 0.001; ns, non-significant. See also Figures S1 and S2.

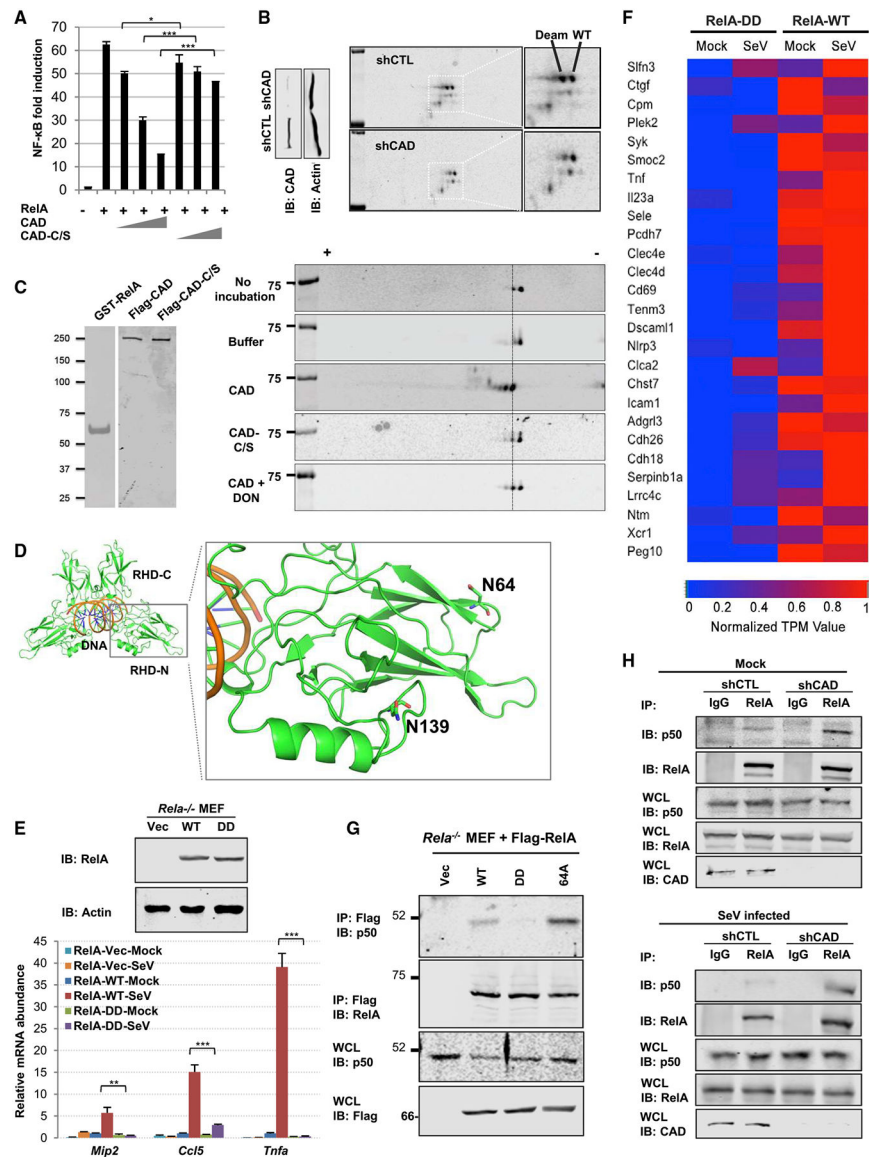


Figure 2. CAD Deamidates RelA to Inactivate NF-κB

(A) NF-κB luciferase reporter assay from 293T cells with increasing amount of a plasmid containing CAD or the enzyme-deficient CAD-C/S.

(B) Immunoblots of whole cell lysates (WCLs) of control (shCTL) or CAD-depleted (shCAD) human HCT116 cells after regular SDS-PAGE (left panels) or two-dimensional gel electrophoresis (2DGE) (right panels). WT and Deam denote wild-type and deamidated RelA, respectively.

(C) Silver stains of purified GST-RelA, CAD, and CAD-C/S (left panel). Immunoblots of *in vitro* deamidation reactions analyzed by 2DGE (right panel).

(D) Structure of the Rel Homology Domain with the deamidated sites, N64 and N139, which locate within two loops of the insertion region. PDB: 1RAM.

(E and F) Immunoblots of WCLs from *Rela*^{-/-} MEFs reconstituted with vector, RelA-WT, or RelA-DD (top panels). The mRNA abundance of *Mip2*, *Ccl5*, and *Tnfa* in reconstituted

MEFs infected with SeV (E). A heatmap representing NF- κ B-dependent gene expression of the reconstituted MEFs (F).

(G) Immunoblots of precipitated proteins and WCLs from reconstituted MEFs as described in (E) that were treated with TNF- α .

(H) Immunoblots of precipitated proteins and WCLs from control (shCTL) or CAD-depleted (shCAD) 293T cells under mock- (top panels) or SeV-infected (bottom panels) conditions.

Data are presented as mean \pm SD. Significance was calculated using two-tailed, unpaired Student's t test. * $p < 0.05$; *** $p < 0.001$; ns, non-significant. See also Figures S3 and S4.

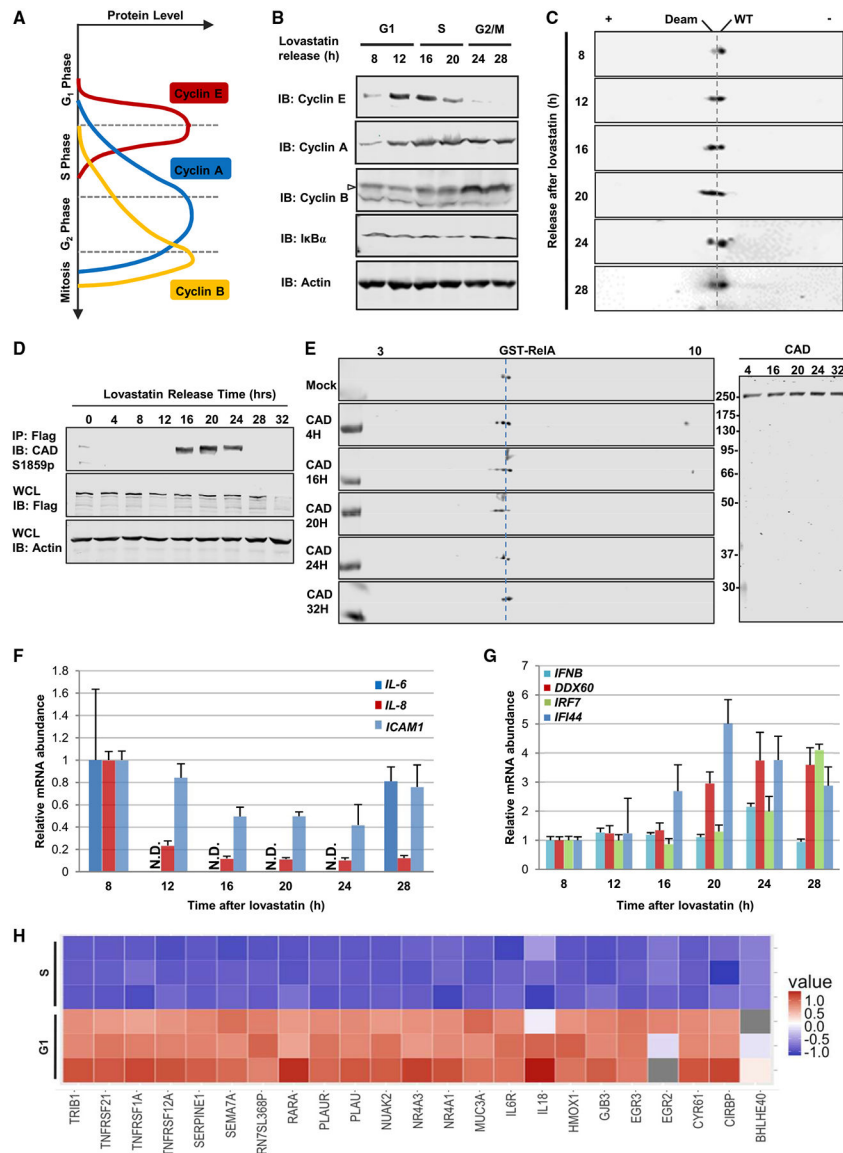


Figure 3. RelA Deamidation and NF- κ B Downregulation Is Cell Cycle-Dependent

(A) Diagram showing distinct cell cycle phases marked by corresponding cyclin expression. (B and C) Immunoblots of whole cell lysates (WCLs) from HCT116 cells released at indicated time points after lovastatin arrest analyzed by regular SDS-PAGE (B) or two-dimensional gel electrophoresis (2DGE) (C). Deam: deamidated; WT, wild-type. (D and E) Immunoblots of precipitated CAD or WCLs from HCT116 Flag-CAD knockin cells (D). Immunoblots of *in vitro* deamidation with precipitated CAD at indicated time points analyzed by 2DGE (E). (F and G) The mRNA abundance of *IL-6*, *IL-8*, and *ICAM1* (F) or *IFNB*, *DDX60*, *IRF7*, and *IFI44* (G) in HCT116 harvested at indicated time after lovastatin arrest. (H) A heatmap showing the relative expression level of representative NF- κ B-responsive genes in HCT116 cells synchronized in S and G1 phase with lovastatin. See also Figures S5 and S6.

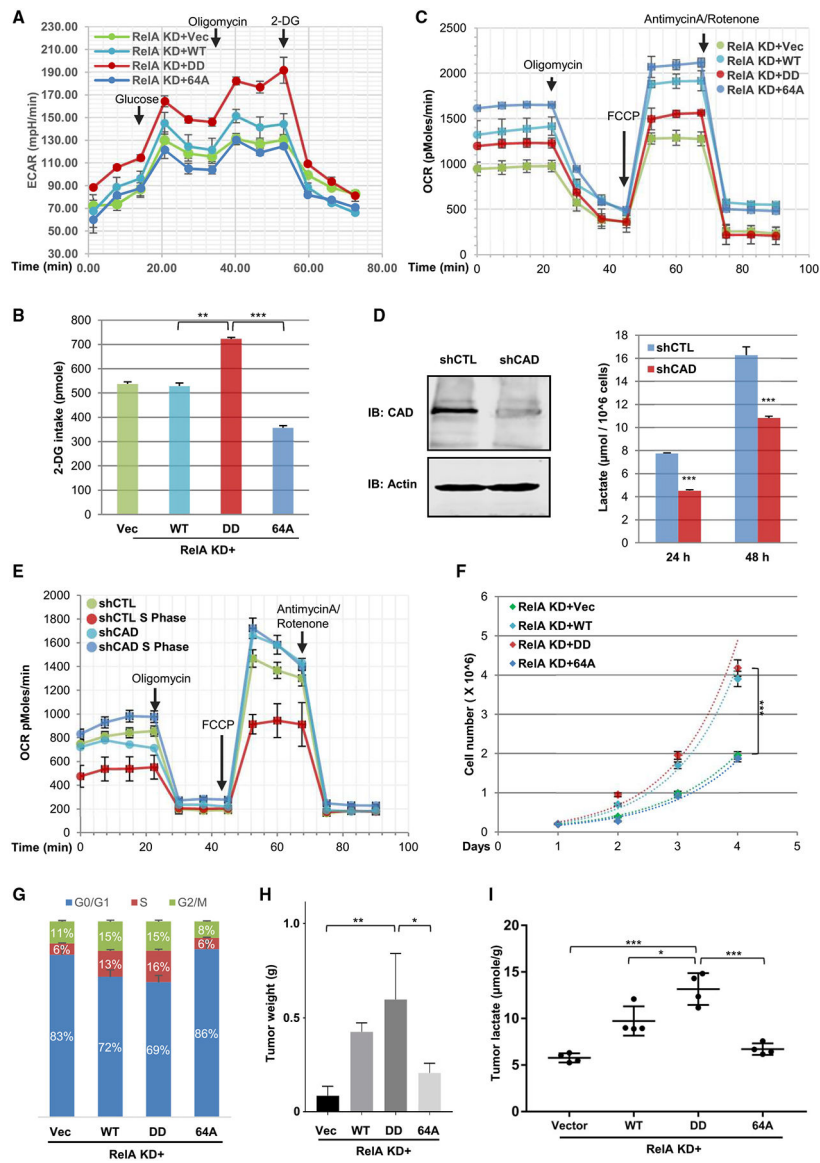


Figure 4. CAD-Mediated RelA Deamidation Is Crucial for Glycolysis and Cell Proliferation
 (A) Extracellular acidification rate recorded from RelA-knockdown (KD) HCT116 cells reconstituted with wild-type (WT), RelA-DD (DD), or RelA-64A (64A) and treated with indicated agents.
 (B) Intracellular 2-DG of reconstituted HCT116 cells as described in (A) determined at 20 min after addition.
 (C) Oxygen consumption rates (OCRs) of reconstituted HCT116 cells as described in (A) treated with indicated agents.
 (D and E) Immunoblots of whole cell lysates of control (CTLs) and CAD-depleted (shCAD) HCT116 cells (left panels) and lactate in the medium measured at 14 h after passaging (D). OCR of control (shCTL) or CAD-depleted (shCAD) HCT116 cells either unsynchronized or S-phase-synchronized with double thymidine block (E).
 (F) Cell number of reconstituted HCT116 cells as described in (A) over 5 days.
 (G) Cell cycle distribution of reconstituted HCT116 cells as described in (A).
 (H) Tumor weight of reconstituted HCT116 cells as described in (A).
 (I) Tumor lactate levels of reconstituted HCT116 cells as described in (A).

(F and G) Cell proliferation of reconstituted HCT116 cells (as in A) analyzed by cell enumeration over time (F) or staining with propidium iodide and flow cytometry (G). (H and I) Tumor weight (H) and lactate levels (I) of tumors derived from reconstituted HCT116 cells as described in (A).

Data are presented as mean \pm SD. Significance was calculated using two-tailed, unpaired (paired for Figure 4F) Student's t test. **p < 0.01; ***p < 0.001; ns, non-significant. See also Figure S7.

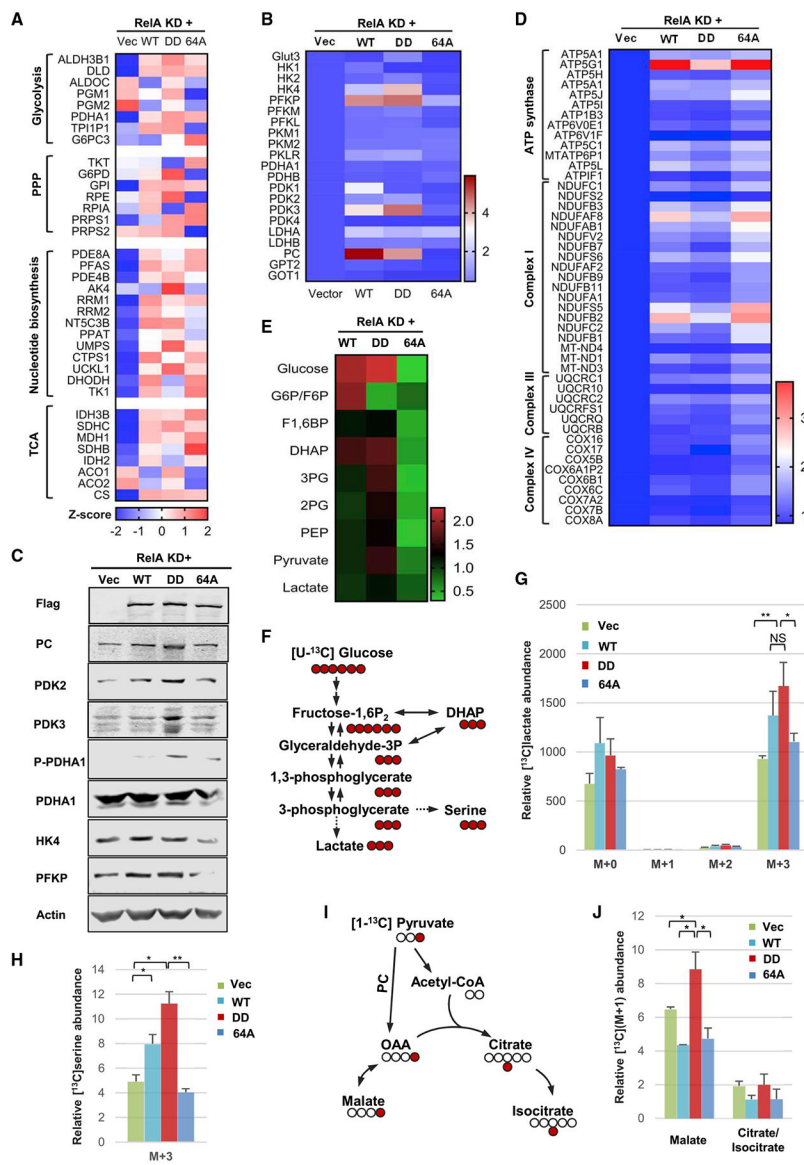


Figure 5. Metabolic Reprogramming by Deamidated RelA

(A–C) A heatmap showing the expression of genes related to glycolysis, the pentose phosphate pathway (PPP), nucleotide and tricarboxylic acid (TCA) cycle (A) of the glycolytic pathway (B) and of mitochondrial oxidative phosphorylation (C), derived from RNA sequencing analysis of RelA-knockdown (KD) HCT116 cells reconstituted with wild-type RelA, RelA-DD, and RelA-64A.

(D) Immunoblots of whole cell lysates from reconstituted HCT116 cells as described in (A). (E) A heatmap showing glycolytic intermediates of reconstituted HCT116 cells as described in (A).

(F–H) Diagram of the isotope labeling of selected glycolytic intermediates using [U-¹³C]glucose (F). Intracellular lactate (G) and glycolytic serine (H) of reconstituted HCT116 (as described in A) traced with [U-¹³C]glucose and analyzed by mass spectrometry. M+a indicates the mass of lactate or serine (+a) universally labeled with [U-¹³C]glucose.

(I and J) Diagram of the conversion of pyruvate to malate reflecting pyruvate carboxylase (PC) activity using [1-¹³C]pyruvate (I) and mass spectrometry analysis of intracellular M+1 malate and citrate (isocitrate) (J).

Data are presented as mean ± SD. Significance was calculated using two-tailed, unpaired Student's t test. **p < 0.01; ***p < 0.001; ns, non-significant. See also Figure S8.

Author Manuscript

Author Manuscript

Author Manuscript

Author Manuscript

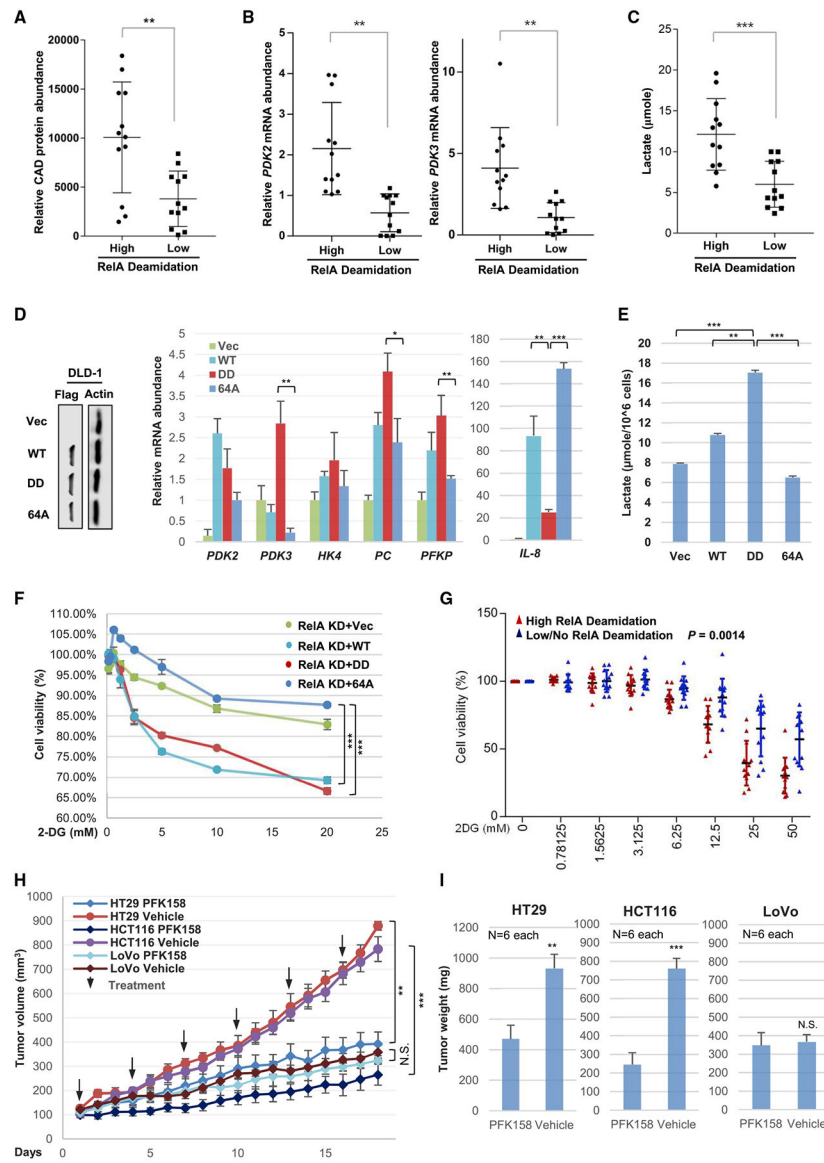


Figure 6. CAD-Mediated RelA Deamidation Is Crucial for Diverse Human Cancer Cells
 (A–C) Human cancer cell lines of the lung, colorectum, and breast were assayed for RelA deamidation and grouped into high- and low-deamidation categories. The mRNA abundance of *CAD* (A), *PDK2* and *PDK3* (B), and lactate concentration (C) quantified in medium at 14 h after passing.

(D and E) Immunoblots of whole cell lysates from DLD-1 colorectal cancer cells, with low levels of CAD and RelA deamidation, which express exogenous wild-type RelA (WT), RelA-DD and RelA-64A (left panels), and relative mRNA abundance of indicated glycolytic genes analyzed by real-time PCR (D). Lactate concentration in medium at 14 h after passing (E).

(F) Cell viability of RelA-knockdown (RelA KD) HCT116 cells reconstituted with wild-type RelA (WT), RelA-DD (DD), or RelA-64A (64A) and treated with 2-deoxyglucose (2-DG).

(G) Cell viability of the panel of human cancer cell lines treated with 2-DG as analyzed in (F). Red and blue dots denote individual data point of cancer cell lines with high and low levels of RelA deamidation, respectively.

(H and I) Tumor growth in mice inoculated with HT29 and HCT116 colorectal cancer cells with high CAD and RelA deamidation, and LoVo with low CAD and RelA deamidation, and treated with vehicle or PFK158 (an inhibitor of PFKFB3, 25 mg/kg) (I), and tumor weight in euthanized mice (J).

Data are presented as mean \pm SD. Significance was calculated using two-tailed, unpaired (paired for Figures 6F–6H) Student's t test. **p < 0.01; ***p < 0.001; ns, non-significant. See also Figures S9 and S10.

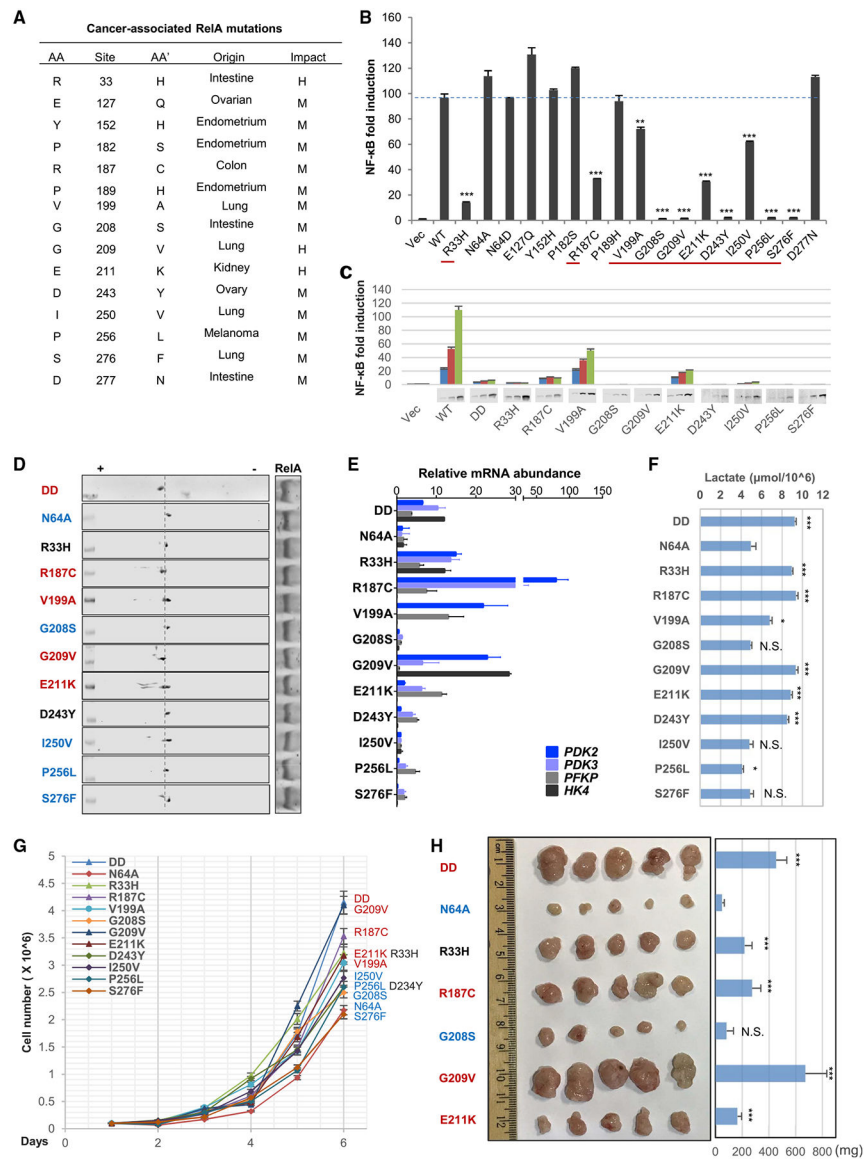


Figure 7. Naturally Occurring RelA Mutations in Human Cancers Predispose RelA to Deamidation and Glycolysis to Fuel Cell Proliferation

(A–C) Naturally occurring mutations in human *RELA* characterized from TCGA public domain (A), NF- κ B activation by RelA mutants analyzed by luciferase reporter assay, with those of reduced NF- κ B activation underlined by red lines (B), and NF- κ B activation of the underlined RelA mutants by luciferase report assay with immunoblots of RelA proteins at the bottom (C).

(D–F) Immunoblots after two-dimensional gel electrophoresis analysis of whole cell lysates from LoVo cells reconstituted with RelA mutants of reduced NF- κ B activation (D). RelA mutants in red indicate elevated deamidation. The mRNA abundance of glycolytic genes analyzed by real-time PCR (E), and lactate production in the medium at 14 h after passaging (F).

(G and H) Cell proliferation (G) and tumor formation in nude mice (H) of reconstituted HCT116 cells as described in (D).

Data are presented as mean \pm SD. Significance was calculated using two-tailed, unpaired Student's t test. **p < 0.01; ***p < 0.001; ns, non-significant.

Author Manuscript

Author Manuscript

Author Manuscript

Author Manuscript

KEY RESOURCES TABLE

REAGENT or RESOURCE	SOURCE	IDENTIFIER
Antibodies		
RelA, F-6, mouse monoclonal	Santa Cruz	Cat# sc-8008; RRID: AB_628017
RelA, C-20, rabbit polyclonal	Santa Cruz	Cat# sc-372; RRID: AB_632037
P50, E-10, mouse monoclonal	Santa Cruz	Cat# sc-8414; RRID: AB_628015
I κ B α , C-21, rabbit polyclonal	Santa Cruz	Cat# sc-371; RRID: AB_2235952
GST, Z-5, rabbit polyclonal	Santa Cruz	Cat# sc-459; RRID: AB_631586
GFP, B-2, mouse monoclonal	Santa Cruz	Cat# sc-9996; RRID: AB_627695
H3, AH3–120, mouse monoclonal	Santa Cruz	Cat# sc-56616; RRID: AB_2263811
Tubulin, B-7, mouse monoclonal	Santa Cruz	Cat# sc-5286; RRID: AB_628411
Cyclin A, H-432, rabbit polyclonal	Santa Cruz	Cat# sc-751; RRID: AB_631329
PCB, E-5, mouse monoclonal	Santa Cruz	Cat# sc-365672; RRID: AB_10851628
PDK3, RR-2, mouse monoclonal	Santa Cruz	Cat# sc-100535; RRID: AB_2268026
CAD, A301–374A, rabbit polyclonal	Bethyl Laboratories	Cat# A301–374A-T; RRID: AB_937745
Cyclin B1, V152, mouse monoclonal	Cell Signaling	Cat# 4135; RRID: AB_2233956
Cyclin E, HE12, mouse monoclonal	Cell Signaling	Cat# 4129; RRID: AB_2071200
RelA S536, 93H1, rabbit monoclonal	Cell Signaling	Cat# 3033; RRID: AB_331284
Phospho-CAD (Ser1859) Antibody, rabbit	Cell Signaling	Cat# 12662; RRID: AB_2750934
Flag, M2, mouse monoclonal	Sigma	Cat# F3165; RRID: AB_259529
β -Actin, Ab8226, mouse monoclonal	Abcam	Cat# ab8226; RRID: AB_306371
Chemicals, Peptides, and Recombinant Proteins		
6-Diazo-5-oxo-L-norleucine (DON)	Sigma	Cat# D2141; CAS# 157-03-9
Human recombinant TNF- α	R&D systems	Cat# 210-TA
Mouse recombinant TNF- α	R&D systems	Cat# 410-MT
Lipopolysaccharides (<i>E.coli</i> O111:B4)	Sigma	Cat# L3023
Lovastatin	LKT Labs	Cat# M1678; CAS# 75330-75-5
(\pm)-Mevalonolactone	Sigma	Cat# M4667; CAS# 674-26-0
Thymidine	Sigma	Cat# T1895; CAS# 50-89-5
Uridine	Sigma	Cat# U3003; CAS# 58-96-8
2-Deoxyglucose	Sigma	Cat# D8375; CAS# 154-17-6
Propidium Iodide	Sigma	Cat# P4170; CAS# 25535-16-4
[U ¹³ C] Glucose	Cambridge Isotope Lab	Cat# CLM-1396
[1- ¹³ C] Pyruvate	Sigma	Cat# 490709; CAS# 87976-71-4
PFK158	SelleckChem	Cat# S8807
Critical Commercial Assays		
Lactate Assay Kit	Sigma	Cat# MAK064
Cell Mitochondria Stress Test Kit	Agilent	Cat# 103010–100
Cell proliferation kit II	Sigma	Cat# 11465015001
Glucose Uptake Colorimetric Assay Kit	Sigma	Cat# MAK083
TRI reagent	Molecular Research Center	Cat# TR 118

REAGENT or RESOURCE	SOURCE	IDENTIFIER
SYBR Green Master Mix	Sigma	Cat# S4438
Human CCL5 ELISA kit	R&D systems	Cat# DRN00B
Human IL6 ELISA kit	Proteintech	Cat# KE00007
Human IL8 ELISA kit	Proteintech	Cat# KE00006
KAPA RNA-seq library kit	Roche	Sequencing.roche.com
Deposited Data		
'Reconstituted' HCT116 RNA-seq data	This paper	GEO: GSE132868
Synchronized HCT116 RNA-seq data	This paper	GEO: GSE132868
'Reconstituted' <i>Rela</i> ^{-/-} MEF RNA-seq data	This paper	GEO: GSE132871
Mendeley Data	This paper	https://doi.org/10.17632/shnf4m8khn.1
Experimental Models: Cell Lines		
HEK293T	ATCC	Cat# ACS-4500; RRID: CVCL_4V93
HCT116	ATCC	Cat# CCL-247; RRID: CVCL_0291
THP-1	ATCC	Cat# TIB-202; RRID: CVCL_0006
<i>Rela</i> ^{-/-} MEF	Dr. Linfeng Chen, UIUC	N/A
MCF-7	Dr. Min Yu, USC	N/A
T47D	Dr. Min Yu, USC	N/A
BT474	Dr. Min Yu, USC	N/A
SKBR3	Dr. Min Yu, USC	N/A
MDAMB231	Dr. Min Yu, USC	N/A
HS578T	Dr. Min Yu, USC	N/A
SW480	Dr. Chengyu Liang, USC	N/A
DLD-1	Dr. Chengyu Liang, USC	N/A
Lim2045	Dr. Chengyu Liang, USC	N/A
RKO	Dr. Chengyu Liang, USC	N/A
HT29	Dr. Chengyu Liang, USC	N/A
Colo26	Dr. Chengyu Liang, USC	N/A
LoVo	Dr. Chengyu Liang, USC	N/A
H1944	Dr. Ite Laird Offringa, USC	N/A
H1975	Dr. Ite Laird Offringa, USC	N/A
H522	Dr. Ite Laird Offringa, USC	N/A
PC9	Dr. Ite Laird Offringa, USC	N/A
H358	Dr. Ite Laird Offringa, USC	N/A
H1648	Dr. Ite Laird Offringa, USC	N/A
H23	Dr. Ite Laird Offringa, USC	N/A
H2347	Dr. Ite Laird Offringa, USC	N/A
HCC827	Dr. Ite Laird Offringa, USC	N/A
BJ5-5ta	ATCC	Cat# CRL-4001; RRID: CVCL_6573
Flag-CAD Knockin HCT116	Home made	N/A
RelA Knockin MEF	Home made	N/A
A-253, ATCC HTB-41	ATCC	Cat# TCP-1012
SCC-15, ATCC CRL-1623	ATCC	Cat# TCP-1012

REAGENT or RESOURCE	SOURCE	IDENTIFIER
SCC-25, ATCC CRL-1628	ATCC	Cat# TCP-1012
FaDu, ATCC HTB-43	ATCC	Cat# TCP-1012
SCC-9, ATCC CRL-1629	ATCC	Cat# TCP-1012
Detroit 562, ATCC CCL-138	ATCC	Cat# TCP-1012
Experimental Models: Organisms/Strains		
Homozygous <i>Foxn1^{mu}</i>	Jackson Laboratory	NU/J 002019
Homozygous <i>Foxn1^{mu}</i> outbred	Jackson Laboratory	J:NU 007850
Oligonucleotides		
Human GATs shRNA	ThermoFisher	N/A
Human UMPS shRNA	ThermoFisher	N/A
qPCR Primers, see Table S1	N/A	N/A
ChIP-qPCR Primers, see Table S1	N/A	N/A
sgRNA Primers, see Table S1	N/A	N/A
Software and Algorithms		
Graphpad Prism Version 7.00	Graphpad	http://www.graphpad.com
FlowJo	Tree Star	http://www.flowjo.com
R	N/A	http://www.r-project.org
Partek Flow Genomic Analysis	Partek	http://www.partek.com
DESeq2	R package	http://bioconductor.org/packages/release/bioc/html/DESeq2.html
clusterProfiler	R package	https://bioconductor.org/packages/release/bioc/html/clusterProfiler.html
HISAT	R package	https://ccb.jhu.edu/software/hisat2/index.shtml
StringTie	R package	http://ccb.jhu.edu/software/stringtie/index.shtml
ggplot2	R package	https://cran.r-project.org/web/packages/ggplot2/index.html
Others		
Sendai Virus (SeV)	Charles River	PI-1, SV
<i>Salmonella Typhimurium</i> wild-type	Dr. Andrew Ouellette, USC	N/A